Recurrence of drought events in Iberia in EURO-CORDEX regional climate projections

Master thesis in meteorology

Benjamin Körner

April 7 2021

INSTITUT FÜR METEOROLOGIE UND KLIMAFORSCHUNG
KARLSRUHER INSTITUT FÜR TECHNOLOGIE (KIT)

Referent:	Prof. Dr. Joaquim Pinto
Korreferent:	Prof. Dr. Andreas Fink

Abstract

Droughts are a common feature of Mediterranean climate. Droughts in consecutive years (recurrent droughts) are a potential driver for land degradation into a less desirable state in the Iberian Peninsula (IP). There is wide scientific agreement on an increase in general drought risk in the Mediterranean with ongoing climate change. The objective of this thesis is to evaluate change in recurrent drought risk in the IP under future climate conditions. An ensemble of 25 high resolution (0.11°) regional climate model simulations from the framework of the EURO-CORDEX project, run under a high greenhouse gas emission scenario (RCP8.5), is used to represent past and future climate conditions. Precipitation data is bias corrected with a simple mulitplicative approach. The model output is analyzed with the Effective Drought Index (EDI) and a total of eight recurrent drought indices. In general, recurrent droughts are projected to become longer and more frequent with a strong increase towards the end of the 21st century. The majority of trends have significant model agreement in the 2021-2050 period and the vast majority of trends have significant model agreement for the 2071-2100 period. While some models project only moderate changes, the majority of models suggests an almost permanent state of drought under future climate conditions. The region of highest recurrent drought risk increase varies with models and also with the choice of index. The results imply severe consequences in the IP under the RCP8.5 scenario. Ecosystems would be under extreme drought stress and substantial adaption strategies would be required to sustain the water supply.

Zusammenfassung

Dürreperioden sind ein häufiges Merkmal mediterranen Klimas. Dürren in aufeinanderfolgenden Jahren (wiederkehrende Dürren) sind ein potenzieller Treiber für Änderungen der Landoberfläche in einen weniger wünschenswerten Zustand auf der Iberischen Halbinsel (IP). Es besteht ein breiter wissenschaftlicher Konsens über eine Zunahme des allgemeinen Dürrerisikos im Mittelmeerraum bei fortschreitendem Klimawandel. Das Ziel dieser Arbeit ist es, die Veränderung des Risikos von wiederkehrenden Dürren auf der IP unter zukünftigen Klimabedingungen zu bewerten. Ein Ensemble von 25 hochauflösenden (0.11°) regionalen Klimasimulationen aus dem Rahmen des EURO-CORDEX-Projekts, die unter einem Szenario mit hohen Treibhausgasemissionen (RCP8.5) laufen, wird verwendet um vergangene und zukünftige Klimabedingungen darzustellen. Der Bias der Niederschlagsdaten wird mit einem einfachen multiplikativem Ansatz korrigiert. Die Modelldaten werden mit dem Effective Drought Index (EDI) und acht wiederkehrenden-Dürre-Indizes analysiert. Im Allgemeinen wird projiziert, dass wiederkehrende Dürren länger und häufiger werden, mit einer starken Zunahme gegen Ende des 21. Jahrhunderts. Die Mehrheit der Trends hat eine signifikante Modellübereinstimmung im Zeitraum 2021-2050 und die große Mehrheit der Trends hat eine signifikante Modellübereinstimmung für den Zeitraum 2071-2100. Während einige Modelle nur moderate Änderungen projizieren, weist die Mehrheit der Modelle einen fast permanenten Zustand der Trockenheit unter zukünftigen Klimabedingungen auf. Die Region mit dem höchsten Anstieg des Risikos wiederkehrender Dürren variiert je nach Modell und Index. Die Ergebnisse implizieren schwerwiegende Konsequenzen in der IP unter dem RCP8.5-Szenario. Die Ökosysteme wären extremen Dürrestress ausgesetzt und und es wären umfangreiche Anpassungsstrategien erforderlich, um die Wasserversorgung aufrechtzuerhalten.

Contents

1 Introduction 1

2 Theoretical Concepts 5
- 2.1 Iberia . . . 5
  - 2.1.1 General circulation . . . 6
  - 2.1.2 Teleconnections . . . 7
  - 2.1.3 Precipitation regime . . . 8
  - 2.1.4 Droughts in Iberia . . . 8
- 2.2 Drought indices . . . 10
  - 2.2.1 PDSI . . . 11
  - 2.2.2 SPI . . . 11
  - 2.2.3 SPEI . . . 12
  - 2.2.4 EDI . . . 12
  - 2.2.5 Recurrent Drought Indices . . . 14

3 Data and methods 15
- 3.1 EURO-CORDEX . . . 15
- 3.2 E-OBS . . . 17
- 3.3 Bias correction . . . 17
- 3.4 Evaluation . . . 18

4 Results 21
- 4.1 Precipitation changes . . . 21
- 4.2 General drought statistics . . . 22
- 4.3 Recurrent drought duration . . . 27
- 4.4 Recurrent drought frequency . . . 31

5 Discussion 37

6 Conclusion 41

A Abbreviations 43

B Appendix 45

Bibliography 56

1 Introduction

Drought is an environmental disaster that has a variety of impacts and is relevant for several disciplines and sectors, such as hydrology, meteorology, geology and agricultural sciences (Mishra and Singh, 2010). In general, drought is depicted by a lack of water in one or more components of the hydrological cycle over a prolonged time period (McKee et al., 1993). While seasonal dryness or aridity are permanent climate features, drought describes a temporary decline in water supply relative to normal conditions. Therefore it can occur in every climate zone, regardless of annual rainfall amount (Wilhite et al., 2014).

The most likely cause for droughts is a reduction in precipitation. Temperature, wind, relative humidity, timing and characteristics of rain can also be driving factors Mishra and Singh (2010). McKee et al. (1993) states that water scarcity can develop in soil moisture, ground water, snowpack, streamflow or reservoir storage. Since those supplies are interchanging with each other, the drought signal propagates in several properties and causes impacts on a range of spatial and temporal scales.

(Fresh)water is a basic human need and important for any sort of life. Therefore, water availability is directly and indirectly listed in the UN's Sustainable Development Goals (UNDP, 2015). The inaccessibility of water resources on the other hand raises fundamental dangers and therein lies the threatening character of droughts. Drought impacts can be assigned to the categories environmental, economic and social (Wilhite, 1992). Examples are damage to animal and plant species, water and air quality, loss of crop and livestock production, costs of water transport or transfer, loss to energy industry or unemployment in drought related sectors.

Direct impacts are usually of biophysical nature, while indirect impacts are rather found in the socioeconomic sector. A lack of precipitation could result in reduced crop yields, which leads to less income for farmers and raised prices, thereby affecting all members of society (Wilhite et al., 2007). Shahbazbegian and Bagheri (2010) state that droughts can trigger a series of reinforcing mechanisms with the potential to economically disrupt a whole region. Adaawen and Schraven (2019) name droughts as cause of desertification and thereby a driving factor for migration, on scales ranging from local to continental. However, indirect impacts can highly depend on the human response to the direct impact (Shahbazbegian and Bagheri, 2010). This highlights the fact that droughts and their impacts can not be seen as only a natural phenomenon, but rather as an interplay between the physical signal and the demand for water by the ecosystem and human activities (Wilhite et al., 2007). It is therefore easy to understand that droughts will influence future political, economic and social trajectories and also that there is great benefit from diagnosing and

predicting droughts and their impacts.

While it is clear that droughts harm several areas of wildlife and human society, it is difficult to quantify those damages. This is because of the number of groups affected, the big spatial extent, the delay in time and problems with assessing the environmental damage (Wilhite, 1992). Subsequently, there is no universal definition of drought satisfying all of its features. Instead, there are various coexisting definitions, that should be used application specific. Mishra and Singh (2010) and WMO (2006) identify the following four:
(i) Meteorological drought is often defined by decreased precipitation over a specified time period. This results in reduced infiltration, runoff, deep percolation, and groundwater recharge. However, increased atmospheric evaporative demand also influences those properties, so temperature, wind and relative humidity might be taken into account as well.
(ii) Agricultural drought is characterized by the soil's ability to meet the water demand for growing crop plants. Therefore, the amount of water infiltrating the soil is of importance as well as the water-holding capacity of the soil.
(iii) Hydrological drought represents an anomaly in surface and sub-surface water supplies. It is not just depending on inflow, but also on the usage of water for a variety of purposes.
(iv) Socio-economic drought describes the interplay between supply and demand for goods that rely on the amount of precipitation.

In the following, meteorological drought in the Iberian Peninsula is further assessed. In this region, droughts are high impact events. Water demand is already close to the natural supply under normal conditions. For this reason, droughts can quickly lead to water scarcity (Iglesias et al., 2009). There is wide agreement that with ongoing climate change, the West Mediterranean is expected to face drought conditions more often during the 21st century and will be a hotspot for droughts (Hartmann et al., 2013; Spinoni et al., 2018).

Vegetation on the Iberian Peninsula is well adapted to dry conditions, as those are found during every summer and drought variability is high in general (Coll et al., 2017). Caldeira et al. (2015) suggests that droughts that last for longer than one year have a highly relevant role. While ecosystems have a high resistance towards droughts that last for a year, it is these recurring droughts that cause big damages. Such extreme dry conditions may drive ecosystems towards critical limits and favor the invasion of foreign species. As a consequence, cork-oak stands, that are common in Mediterranean-type climates, could transition into less desirable shrublands.

From this, the question arises whether recurring droughts in the Iberian Peninsula will be more frequent and longer under future climate conditions. This is further decomposed: What are the changes in mean conditions and variability? What are the characteristics of drought events? Is the picture consistent among several climate projections?

Model output from an 25 regional climate projections is used to investigate these issues, for a reference period from 1971-2000 and future time periods from 2021-2050 and 2071-2100. In doing so, this thesis is aiming to present a robust assessment of future risk for recurring droughts

in the Iberian Peninsula. Chapter 2 provides theoretical background. Chapter 3 introduces the data and the methods that are applied. Chapter 4 contains the results of the research. Chapter 5 discusses the results and chapter 6 is summarizing the conclusions.

2 Theoretical Concepts

2.1 Iberia

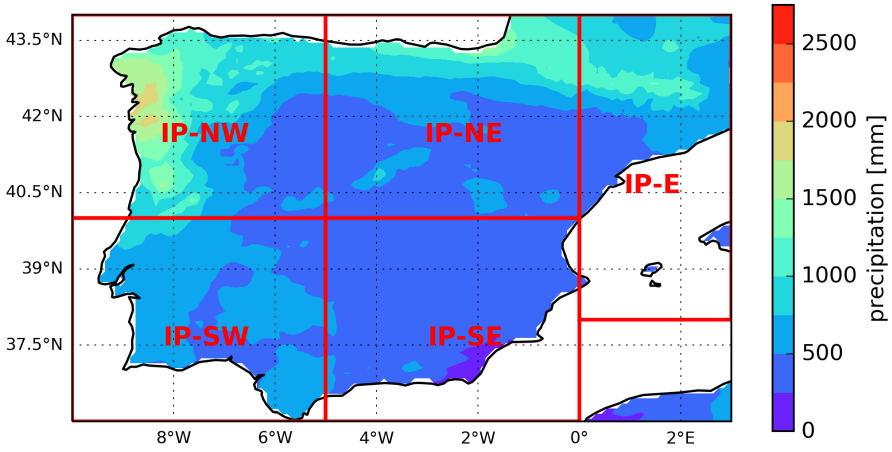

Figure 2.1: Climatological annual precipitation sum in the Iberian Peninsula (in *mm*). Values of E-OBS V20e for the 1971-2000 period. Map section displays the area used for analysis of the IP. Red boxes display subregions of the IP. Regions are: IP (36°N to 44°N, 10°W to 3°E), IP-NW (40°N to 44°N, 10°W to 5°W), IP-SW (36°N to 40°N, 10°W to 5°W), IP-NE (40°N to 44°N, 5°W to 0°E), IP-SE (36°N to 40°N, 5°W to 0°E), IP-E (38°N to 44°N, 0°E to 3°E).

The Iberian Peninsula (IP) is located in the South West of Europe. Distributed over the countries of Spain, Portugal, Andorra and the British enclave Gibraltar lives a population of more than 50 million people. It is surrounded by the Atlantic Ocean and the Mediterranean Sea. The IP has three major river basins, namely the Ebro, Douro and Tejo. High mountain areas are the Galician and Cantabrian mountains along the northern coast, the Pyrenees along the border of Spain and France, the Sistema Central and the Sistema Iberico in the inland and the Baetic System in the South East. Automotive industry, agriculture and tourism are important economic sectors.
The IP has a high variability in spatial rainfall distribution. Fig. 2.1 displays annual precipitation sum in the IP for the 1971-2000 period. Data is from the E-OBS data set (Cornes et al., 2018), that is described in detail in section 3.2. Areas in the North West receive annual rainfall amounts of up to 2000 *mm*. Along the coast in the North, in the neighbouring mountain ranges and the Pyrenees at the French border, mean annual precipitation is around 800 *mm*. At the western coast, rainfall rates are decreasing towards the South, lying at 500 $mm/year$ in Portugals southernmost Algarve region. For the central part, typical values are around 400 $mm/year$ with the exception of the more mountainous areas. The driest region of the IP is at the southeastern coast, where annual precipitation is less than 300 *mm*. The complete map section in Fig. 2.1 is the region used for analyzing values for the whole IP. The red boxes display subregions that are defined for the further regional analysis.

The annual precipitation cycle (not shown) is very pronounced with almost no precipitation during summertime and the highest values in winter. In the western part of the IP, there is a clear maximum of precipitation in wintertime and low values in summertime, even in the wettest regions. Towards the East, the rainfall has a bimodal characteristic, with maxima in spring and autumn. However, winter still has more precipitation than summer.
Esteban-Parra et al. (1998) state that annual precipitation sums are mostly related to rainfall between September and May. Winter is the most important season for most parts of the IP, however autumn is more important for the East. Caldeira et al. (2015) confirms this, showing that precipitation anomalies in the South West of the IP develop mainly in the winter half year.

2.1.1 General circulation

The role of the general circulation for climatic conditions in the IP is discussed in the following. The general atmospheric circulation is driven by the spatial differences in insulation. It is shaped by the rotational speed of the earth, land sea distribution and orographical features.
The Hadley cell is a thermally direct circulation cell, balancing the maximum of insulation in the tropics with the areas further poleward. The radiative heating causes upward motion near the insulation maximum, marking the Intertropical Convergence Zone. The condensation of moisture results in the release of latent heat and high rainfall amounts. At the top of the troposphere, the high pressure causes poleward outflow. The radiative cooling is resulting in subsiding motion, creating the subtropical anticyclones and suppressing convection and precipitation. This process creates the aridity in subtropical regions surrounding the tropics. The low level outflow of the subtropical high streams both equatorward and poleward. The poleward branch meets colder polar air at the polar front. The strong gradient in temperature and the above lying polar jet create baroclinic instability, which generates the mid-latitude cyclones. Cyclones and the associated frontal systems dominate precipitation patterns in the mid latitudes, especially in winter (Buchal and Schönwiese, 2010).
The IP is situated at the border region of these two regimes. Circulation patterns shift poleward in summer and equatorward in winter, hence the low precipitation amounts in summer and the higher amounts in other seasons.
In the fifth Assessment Report of the Intergovernmental Panel on Climate Change (IPCC), (Hartmann et al., 2013) suggest an poleward expansion of the Hadley circulation in the second half of the past century, but the confidence in trends is low due to uncertainties in the data sets. Also they stress that trends are are superimposed with large natural variability in circulation strength. (Collins et al., 2013) state that the Hadley cell is likely to widen by the end of the 21st century. Further, they connect decreases in runoff with this change in general circulation.
Several studies discuss the relationship of circulation changes and precipitation decrease in the Mediterranean in detail. Abnormal anticyclonic flow anomalies over the Mediterranean are found in in CMIP5 global simulations for the 2021-2040 period by (Seager et al., 2014) and in regional climate simulations for the 2071-2100 period by (Tuel et al., 2021), both for the RCP8.5 scenario. Seager et al. (2014) additionally detect the precipitation decreases to be a product of increased mean flow moisture divergence rather than decreased eddy moisture moisture flux convergence. Putnam and Broecker (2017) state that global warming is likely to cause circulation patterns to shift northwards. The associated northward displacement of the North Atlantic winter polar jet

and storm track would cause reduced precipitation in the Mediterranean. However, Brogli et al. (2019) find that changes in Hadley cell extent in summer in the European sector are weak and do not agree in sign among different climate models. Summertime precipitation decreases are therefore not directly related to a possible hadley cell expansion. Furthermore, they conclude that these changes are caused by an increase in atmospheric stability and only to a minor degree by the mean state of the circulation. In wintertime however, precipitation decreases are mostly related to changes in the mean state of atmospheric circulation.

Overall, the response of the general circulation to climate change is assumed to be the main driver of precipitation changes in the Mediterranean, even though there are several perspectives assessing this relationship.

2.1.2 Teleconnections

Teleconnections describe large scale atmospheric modes (Trigo et al., 2004).

The North Atlantic Oscillation (NAO) depicts the strength of the climatological pressure dipole between the Atlantic mid latitudes (Icelandic low) and the subtropical Atlantic (Azores anticyclone). It is the most prominent mode of variability in the northern hemisphere, especially in the winter half year (Comas-Bru and McDermott, 2014). Precipitation in the IP is depending on moisture advection, driven by the large scale circulation. The NAO therefore has a great potential in explaining precipitation variability (Trigo et al., 2004). In the past, several station based indices were introduced that were closely related to the NAO (Hurrell et al., 2003). Other indices used averaged westerly wind speed in the Atlantic basin. Modern approaches include principal component time series of sea level pressure (Hurrell et al., 2003).

The positive phase is characterized by an increased pressure gradient between the Arctic and the Subtropics and an enhanced zonal flow in the Atlantic basin, while the negative phase is characterized by a decreased pressure difference and weaker than normal zonal flow (Comas-Bru and McDermott, 2014). The positive phase of the NAO shows a dipole pattern in precipitation anomaly, with higher than normal values in the northern Atlantic and northern Europe and below average values in southern Europe. In the negative phase, this pattern is reversed (Trigo et al., 2004). In analogy, Trigo et al. (2004) find significant negative correlations between the NAO and river discharge in the Douro, Tejo and Guadiana basins, as well as for potential hydroelectric power generation.

The second teleconnection of high importance for precipitation in europe is the East Atlantic pattern (EA). Wallace and Gutzler (1981) identify the EA as a teleconnection in in the 500 hPa geopotential height field, with three centers, located to the West of the British Isles, over the Canary islands and near the Black sea. The EA is commonly identified as the second leading Empirical Othorgonal Function (EOF) of sea level pressure in the North Atlantic basin (Moore et al., 15 Apr. 2013). A positive EA index indicates a higher than normal 500 hPa height over the British Isles and a lower than normal 500 hPa height at the other two locations. A negative EA index is affiliated with a pattern of opposite sign. This has implications on the zonal flow and precipitation in western Europe, which is negatively correlated with the EA (Comas-Bru and McDermott, 2014).

2.1.3 Precipitation regime

Several studies go more into detail concerning precipitation patterns in the IP by using statistical downscaling approaches. This allows an understanding of the connection between local precipitation patterns and the large scale flow.
Goodess and Jones (2002) relate Iberian rainfall station data from 1958-1997 to circulation weather types. The results show that cyclonic weather types cause more rainfall than anticyclonic types. The effect of directional weather types is depending on the location. Westerly circulation types are the most important types for rainfall for most of the IP, with the exception of the South East, where precipitation is mostly corresponding with an eastern and southeastern circulation.
Establishing relationships of precipitation and teleconnection indices is another possibility for statistical downscaling. Rodriguez-Puebla et al. (1998) analyze annual precipitation variability in the IP by identifying the four leading EOFs of annual precipitation in station rainfall data from 1949 to 1995. The first leading function, accounting for 33 % of total variance, is correlated with the April EA. The second leading function, associated with the NAO, explained a variance of 19 %. The third and fourth leading functions, accounting for 14 % and 13 % of variance, are correlating with the October Southern Oscillation Index of the previous year and the December Scandinavian pattern.
EOF analysis is also suited to identify coherent spatial rainfall patterns. Esteban-Parra et al. (1998) investigate precipitation records in Spain for the 1880-1992 period. The first rotated EOF pattern is associated with the South and the interior of Spain, the second and third EOF patterns are related to rainfall at the Mediterranean and Cantabric coast respectively. The principal component (PC) time series shows significant correlations for most of the identified regions and seasons, but with strongest correlations in winter. The PC time series and the mean sea level pressure at Ponta Delgada, which is linked to the Azores anticyclone, are negatively correlated, again with the strongest correlations in winter and for the first EOF.
These downscaling approaches allow for the establishment of significant correlations with precipitation. Even though they can not completely explain precipitation variability, they underline its strong dependence on the large scale flow.

2.1.4 Droughts in Iberia

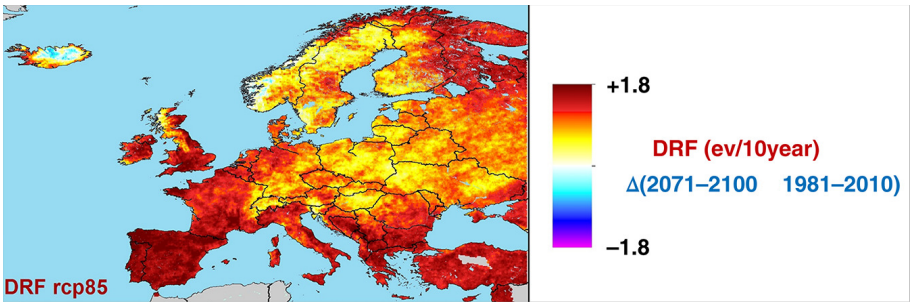

Figure 2.2: Projected changes in drought frequency under the RCP8.5 scenario for an ensemble mean of 11 regional climate projections (in number of events per decade). Figure 3 in (Spinoni et al., 2018).

The Mediterranean is particularly vulnerable to droughts, as water demand is already close to natural supply under normal and quickly exceeds natural supply in case of water scarcity (Iglesias

et al., 2009). This is reflected in a high socioeconomic risk associated with droughts (Gu et al., 2020).

Historically, droughts are a common feature on the IP. Coll et al. (2017) describe historic drought variability and trends in the IP using station data from 1906-2010. Variations on decadal scales can be detected, with rather dry periods in in the 1920s, 1940s and 1950s, and from the 1980s ongoing. The single heaviest drought events occured in 1945, 1995 and 2005. While there is no significant trend found in terms of precipitation, the SPEI, which is a precipitation and temperature dependent drought index, shows a significant drying trend for many stations.

A detailed overview of the causes and impacts of the 2004/2005 drought is presented in García-Herrera et al. (2007). From a Eulerian perspective, the circulation in the 2004/2005 winter was dominated by dry weather types. From a Lagrangean perspective, a striking absence of storm tracks over the IP due to blocking is detected. Extreme low rainfall amounts in the winter season, especially in the southern part of the IP, led to a precipitation deficit. The drought resulted in a reduction of hydroelectric power production of 60 % and a reduction of cereal yield of 40 %.

In the fifth Assessment report of the IPCC, Hartmann et al. (2013) finds that droughts are likely to have increased in the Mediterranean since the middle of the last century. Also, Collins et al. (2013) concludes dryer conditions in the Mediterranean to be likely with ongoing climate change, even more as this signal is reproduced already in earlier model generations (Orlowsky and Seneviratne, 2012) and was already expected in the second IPCC Assessment report (Reilly et al., 1995).

Projected changes in drought frequency and severity in the Mediterranean for the 21st century are assessed in (Spinoni et al., 2018), using regional climate projections. On the IP, for both the RCP4.5 and RCP8.5 scenario, droughts are believed to occur oftener and increase in severity, but with a more pronounced change under the RCP8.5 scenario. The changes of drought frequency under the RCP8.5 scenario of the ensemble mean are shown in Fig. 2.2. High agreement on the trend direction among the model projections highlights the robustness of these findings.

Decreases in precipitation are a main driver of drought trends (Seager et al., 2014). Santos et al. (2016) use a weather type classification for the North Atlantic and West European sector to relate declining precipitation sums in RCP8.5 projections to changes in circulation. The alteration in rainfall can mostly be assigned to a decrease in the rainy weather types and an increase in dry weather types, even though a weather type independent drying signal is also identified.

Addressing drought projections on a smaller regional scale, Guerreiro et al. (2017) analyzed droughts in CMIP5 global climate models in the three international Iberian river basins under the RCP8.5 scenario. The models agree in an intensification of drought conditions, while there is dissent in the extent of that increase. They note that models that reproduce the large scale flow well do not necessarily have a high skill in depicting historical drought conditions. Furthermore, models that show a different skill in simulating historic droughts, project similar drought characteristics for the future. Due to these inconsistencies, they encourage to not disregard single models but to use the biggest ensemble possible when assessing drought in the IP in climate projections.

While there is general agreement in the scientific community on an increase in drought risk in the IP, a deeper understanding of characteristics and consequences is required for appropriate mitigation actions (Hamdy et al., 2008).

2.2 Drought indices

As mentioned before, drought in a meteorological sense is depicted by a decrease of moisture flux from the atmosphere into the soil, usually caused by a lack of precipitation.

Meteorological drought stands at the beginning of the temporal evolution of drought events and is therefore also the precursor for drought related damages (Mukherjee et al., 2018). The monitoring of the hydrological cycle can therefore provide valuable information to decision makers and help mitigate drought impacts on short and long term (McKee et al., 1993). Drought indices (DI) have been developed to act as such a supportive tool. They allocate relevant hydroclimatic variables and describe the state of drought in a single numeric value.

Of the DIs developed so far, one can broadly differ between precipitation based indices and those that take into account more components of the hydrological cyclce.

DIs that include only precipitation are based on the assumption that precipitation is the main driver for drought variability. Because they only depend on precipitation, data collection is relatively easy. Also, they have a relatively easy computation process. The most prominent example of precipitation based DIs is the Standardized Precipitation Index (SPI), which is operationally used in drought monitoring (McKee et al., 1993).

DIs that incorporate more variables than precipitation aim at reenacting a water balance model (Palmer, 1965). The historically most established of these indices is the Palmer Drought Severity Index (PDSI), which is regarded as a landmark in drought monitoring (Palmer, 1965). As mentioned before, the evolution of drought also depends on atmospheric evaporative demand (AED) and geological properties. Therefore, those DIs additionally include variables like temperature, evapotranspiration, wind speed and soil water holding capacity. That can improve the performance of the DI if the variability of the other variables are of similar magnitude than that of precipitation or if they follow a temporal trend (Vicente-Serrano et al., 2010). This performance enhancement comes with the cost of a more complex computation and higher requirements for the availability and quality of data. This is highlighted in the representation of AED, which often is done by estimating the potential evapotranspiration (PET). There are several methodologies to obtain PET, with the Thornthwaite (Thornthwaite 1948) and Penman-Monteith (Howell and Evett, 2004) equations being the most prominent ones. The Thornthwaite equation only incorporates monthly mean temperature. The Penman-Monteith equation uses more variables as input data, namely daily mean temperature, wind speed, relative humidity and solar radiation. DIs differ with the method of PET calculation, and the Penman-Monteith approach is generally performing better than the Thornthwaite approach (Stagge et al., 2014). However, requirements for data availability and quality are higher for the Penman-Monteith equation, which reduces its applicability. Additionally, Milly and Dunne (2017) warn that most of the commonly used PET methods tend to overestimate the climate change driven increase in PET.

With the variety in impacts, there is hardly a DI that is satisfying for every application. Instead, a DI has to be found that is suitable for the specific case (WMO, 2006). Relevant prospects of this thesis are the duration and frequency of recurrent droughts (RD). It is desirable to use a DI that requires low computational effort and few input variables, since the model ensemble is large. A special focus should be on soil moisture, because it is the water source for plants and therefore the

key component in ecological drought impacts. In the following sections, there will be an overview of the most used DIs and the ones selected for this thesis.

2.2.1 PDSI

The Palmer Drought Severity Index (PDSI) was developed in Palmer (1965) and is historically the most common DI. It is based on a physical water balance model, including precipitation, potential evapotranspiration (PET) and a 2-layer bucket type model for soil moisture. In this model, the PDSI is a standardized value for the required amount of precipitation needed to return to normal conditions.
The PDSI was calibrated with the climatic circumstances of the Central USA. As a result, PDSI values in different locations are not comparable. To overcome this problem, Wells et al. (2004) developed the self calibrated PDSI ($PDSI_{sc}$), which adjusts to the location it is applied at. Another point of critic is that the PDSI has shown to have an inherent time scale of about 12 months. Therefore it is not capable of detecting droughts on shorter timescales (McKee et al., 1993), albeit the un-smoothed Z-Index , which is computed in the process, could be used for that purpose. The PDSI is using PET to estimate AED, which comes along with problems discussed before.
Nonetheless, the PDSI and it's variations are widely used in drought monitoring. Mukherjee et al. (2018) use the $PDSI_{sc}$ to investigate drying trends in a warming climate. The PDSI is used operationally for the North American drought monitor (NOAA and NCEI, 2002).

2.2.2 SPI

The Standardized Precipitation Index (SPI) was introduced by (McKee et al., 1993) with the goal to express the deviation of precipitation from the climatological normal in a probabilistic way. The only input variable for the SPI is the precipitation sum over a specified time range. Time ranges are usually multiplicities of 1 month. They are chosen to match the characteristic timescale of the processes of interest.
To calculate the SPI, first a reference period has to be chosen that ideally has an at least 30 years long record of precipitation. Applying the moving average of the specified timescale produces the reference sample. The goal is to assign measured precipitation values to a probability in units of standard deviation. However, precipitation sums for periods of 12 months or less are not normally distributed. Therefore, precipitation from the reference period is fitted to a Gamma function. The estimated inverse normal is then used to create a normally distributed probability density of the precipitation deviation, with a mean of 0 and a standard deviation of 1. That way, a probability with respect to the reference data can be assigned to any measured precipitation value. The standardization also allows to compare droughts at different locations and climates.Negative SPI values depict abnormal dry conditions, with moderate drought at values below -1, severe drought when smaller then -1,5 and extreme drought when smaller then -2. The simplicity of the computation is the big advantage of the SPI. It is relatively easy to create continuous time series, since precipitation is the only required input variable.
(Mukherjee et al., 2018) state that the SPI is of limited use to quantify the impact of climate change on droughts. Because of the missing representation of temperature it can not account for the trend in increasing AED. (Byun and Kim, 2010) criticized the simple accumulation of precipitation over

time. To assess (in particular temporal) drought characteristics, a weighting of the past rainfall events would be desirable, because strong rainfall events in the past can cause a rapid decrease in the SPI value when the moving accumulation period shifts beyond those events. Another problem is that current SPI values are only available at the end of the month (Deo et al., 2017), even though changes in the state of drought may have already occurred.

Overall, the SPI can give a good estimate of drought conditions while having low data requirements. Therefore, Hayes et al. (2011) proposed the SPI to be the internationally preferred index for meteorological drought. Also, the SPI is used operationally in the North American drought monitor (NOAA and NCEI, 2002).

2.2.3 SPEI

The Standardized Precipitation Evapotranspiration Index (SPEI), proposed in (Vicente-Serrano et al., 2010), assesses drought by incorporating precipitation and PET. This way it offers a possibility to characterize drought while considering the dependency on AED.

The computation of the SPEI is built on the difference between precipitation and PET (P-E). With this value, a calculation process similar to the SPI is carried out. The difference is that P-E here is fitted to a log-logistic distribution. In analogy, SPEI values are classified in drought severity categories. The SPEI is aiming to combine the sensitivity of the PDSI (to temperature amongst others) with the simplicity in calculation of the SPI. However, the SPEI is depending on PET and the weaknesses of this proceeding have already been discussed.

The SPEI presents an opportunity to assess drought risk, especially under climate change conditions, given there is robust data available. Therefore it is being used to analyze drought trends related to climate change (Coll et al., 2017; Vicente-Serrano et al., 2014).

2.2.4 EDI

EDI value	Classification
EDI >2.0	Extremely wet
1.5<EDI≤2	Severely wet
1.0<EDI≤1.5	Moderately wet
0<EDI≤1.0	Mildly wet (Normal)
−1.0<EDI≤0	Mild drought (Normal)
−1.5<EDI≤−1.0	Moderate drought
−2.0<EDI≤−1.5	Severe drought
EDI ≤−2.0	Extreme drought

Figure 2.3: Effective Drought Index (EDI), drought intensity classification. Table 1 in (Lee et al., 2014).

The Effective Drought Index (EDI) was introduced by (Byun and Wilhite, 1999) with the goal to improve monitoring of drought properties compared to existing indices. While using precipitation

as only input variable, a weighting function is applied to simulate the loss of water in soil moisture over time.

Calculating Effective Precipitation (EP) is the first step in computing the EDI. EP for a given date is the accumulated past precipitation, weighted according to the time lag.

$$EP_i = \Sigma_{n=1}^{i} \left[(\Sigma_{m=1}^{n} P_m)/n \right] \tag{2.1}$$

with the precipitation of m days before P_m and the duration of summation i. Usually 365 days are chosen for i, which seems appropriate for this application. Because the water household in the IP strongly depends on the winter half year (Caldeira et al., 2015), the EP on any day in summertime should have the complete previous rainy period (and therefore the past year) weighted in.

$$MEP_{cd} = \Sigma_{cd=1}^{30} EP_{cd} \tag{2.2}$$

MEP_{cd} is the 30 year mean of EP on a specific calendar date.

$$DEP = EP - MEP_{cd} \tag{2.3}$$

DEP is the deviation of EP from MEP_{cd}.

$$EDI = DEP/SD(DEP_{cd}) \tag{2.4}$$

DEP normed with the standard deviation of DEP on that calendar date $SD(DEP_{cd})$ then produces the EDI value of a given date. Therefore, the unit of EDI is 'standard deviation'. This standardization allows for a comparison of drought at different locations, regardless of their climate baseline and variability.EDI values are categorized in terms of severity in Fig. 2.3, similar to the SPI and SPEI.

The EDI is found to be suited to assess historical drought characteristics (Deo et al., 2017; Lee et al., 2014) and model soil moisture (Khodayar et al., 2015). Moreover, it is used to detect changes in droughts under future climate scenarios in (Kamruzzaman et al., 2019) and (Kim and Byun, 2009).

With having daily values, the EDI is able to detect droughts on a variety of timescales (Byun and Kim, 2010). The EDI allows the determination of drought onset and end of drought by counting the consecutive days with EDI < -1. Development of drought is monitored close to real time whereas for other DIs, a value can only be determined by the end of a month, which may result in a costly loss of time for decision makers in the case a developing drought.Vice versa, a single heavy rainfall event potentially ends a dry period, which then also is detected in the EDI time series. Because precipitation is weighted, the EDI is able to resemble the filling up in case of precipitation events as well as the slow decrease with time in storage of water bodies. Therefore, the EDI delivers a more accurate representation of drought onset, opposed to DIs that use a moving average (Byun and Kim, 2010). Additionally, since the EDI has daily precipitation as only input variable, data requirements are low compared to DIs that incorporate PET. However, it should be pointed out, that even though the EDI accounts for the water loss of water bodies over time, it does not actually physically resolve these processes. This is especially true in the context of climate change, where the increasing temperature trends also increase AED.

Considering all advantages and disadvantages, the EDI is chosen to assess drought characteristics in this thesis because:
• Possible overestimation of the climate change induced drying trend resulting from PET calculations (Milly and Dunne, 2017) is avoided.
• Only daily precipitation is needed as input variable, reducing the computational effort from the background of a big model ensemble and bias correction.
• EDI outperforms SPI, which has the same above mentioned advantages (Byun and Kim, 2010).

2.2.5 Recurrent Drought Indices

A total of eight DIs is introduced in (Moemken and Pinto, 2021) to assess RDs. The concept is based on the Consecutive Dry Days (CDD) that is listed as climate change index by the 'Expert Team of Climate Change Indices' (Peterson, 2005; Zhang et al., 2011; Van Engelen et al., 2008). The RD indices differ in the examined drought property, the number of spatial dimensions, and the definition of drought years. This guarantees an examination of RDs from various perspectives, increasing the robustness of the results.
First, maximum duration indices are distinguished from frequency indices. The maximum duration indices identify the longest streak of drought years in a time series. The frequency indices count the number of events with at least two consecutive drought years. Second, indices with one spatial dimension apply drought criteria to a defined area and produce a single numerical value. Indices with two spatial dimensions apply drought criteria to single grid points and produce a two dimensional field. The drought definitions are mentioned in detail in the description of the indices.
The Recurrent Dry Year Index (RDYI) is a maximum duration index applied at a single grid point. A dry year is identified if the annual precipitation sum is below 65 % of the climatological value. The Number of Dry Periods (NDY) is the respective frequency index to the RDYI. Note that this definition detects dry years instead of drought years at single grid points (Moemken and Pinto, 2021).
The Consecutive Drought Year Index (CDY) is a maximum duration index applied for an area. Drought years are identified if annual precipitation sum is below 65 % of the climatological value at least at 10 % of grid points in that area. The Number of Drought Periods (NDP) is the corresponding frequency index.
The Consecutive Drought Year Index based on EDI at single Grid Points (CDY_EDI_GP) assesses maximum RD duration at a single grid point. A drought year is identified if EDI is less or equal -1 at least on 90 days of the year. The Number of Drought Periods based on EDI at single Grid Points (NDP_EDI_GP) counts the number of events with at least 2 years length under this definition.
The The Consecutive Drought Year Index based on EDI (CDY_EDI) is a maximum duration index applied for an area. Drought years are identified if the spatial mean of EDI in that area is less or equal -1 at least on 90 days of the year. The Number of Drought Periods based on EDI (NDP_EDI) is the complementing frequency index to CDY_EDI.

3 Data and methods

Climate models simulate the evolution of the climate system or some of its components over time (Kirtman et al., 2013). By applying an external forcing and boundary conditions, the simulation can be used to resemble the climate of specific periods. However, the results do not represent the exact state of the system at a particular point in time, but rather possible trajectories under the given conditions. This allows a statistical description of the climate of a certain period. Therefore, climate simulations can act as a tool to estimate the expected changes in a future climate, and then are called climate projections (Kirtman et al., 2013).
This chapter is presenting the climate model data that is chosen for this thesis, the observational data that is acting as reference, the applied bias correction method and an evaluation of this method.

3.1 EURO-CORDEX

The model data for this study of change in drought conditions was generated in the framework of the Coordinated Regional Downscaling Experiment (CORDEX), because the big number of model ensemble members increases the robustness of the results. Giorgi et al. (2008) introduces the CORDEX project and examines its necessity: Global climate models (GCM) are able to simulate the general circulation, however, relevant processes at a finer scale, for example orographically forced flow and resulting precipitation patterns, can not be reproduced (Ludwig et al., 2019). Giorgi et al. (2008) further states, that in order for policy makers to adapt to the risks of climate change, it is important to quantify its impacts on a regional to local scale. Subsequently, GCMs are not capable of satisfying the demand for climate impact information. Downscaling techniques are an attempt to meet this demand. Dynamical downscaling implements simulations at finer resolutions on limited area or for selected time slices. Broadly, statistical downscaling relates large scale predictors to regional scale predictants and uses the output from climate simulations. The CORDEX project is an effort to standardize such downscaling efforts in order to improve regional climate downscaling, produce improved multi-model high resolution climate change information for impact and adaption work and stimulate communication between climate modelers, the downscaling community and end-users (Giorgi et al., 2008).
The dynamical downscaling strategy applied in EURO-CORDEX is one-way nesting. That means a GCM is generating the global fields of meteorological variables and a regional climate model (RCM) is run on a smaller domain, with the boundary conditions fed from the GCM (Giorgi et al., 2008). However, there is no feedback from the RCM to the GCM, hence it is called one-way nesting. While this feedback could potentialy improve results, the computational cost is much lower for one-way nesting, as the field of the GCM is not altered and has to be computed only once, regardless of the number of RCMs it is to be paired with (Li et al., 2016).

The Coupled Model Intercomparison Project 5 (CMIP5) is a set of coordinated global climate model experiments to be carried out in the lead up to IPCC Assessment Report 5 (Taylor et al., 01 Apr. 2012). All climate projections of CMIP5 are run under specific greenhouse gas concentration scenarios. These so called Representative Concentration Pathways (RCP) are developed under different assumptions of future political and economic human behaviour (Meinshausen et al., 2011). They are named after the value of increased radiative forcing due to greenhouse gas emissions in 2100. The RCP8.5 scenario therefore has an increased radiative forcing of 8.5 W/m^2 by the end of the century. RCP8.5 was designed to be a non-mitigation, high emission baseline scenario. It should therefore not be interpreted as an business-as-usual, but rather as an worst-case scenario (Hausfather and Peters, 2019). Whether the recent developments in climate and energy politics decrease the likelihood of RCP8.5 is not evaluated in this thesis. However, data availability in EURO-CORDEX simulations is biggest for RCP4.5 and RCP8.5, and recent emission trends are closer to RCP8.5 than to RCP4.5 (Schwalm et al., 2020). For this reason, RCP8.5 is the scenario chosen for the further analysis.

To assess drought changes in the IP, data from the European domain (EURO-CORDEX)is chosen. While there is also a Mediterranean domain, there are more data sets available for EURO-CORDEX, and since the IP is in the very West of the Mediterranean, the EURO-CORDEX domain has a bigger part of the upstream area covered by the high resolution RCM. The finest resolution available for EURO-CORDEX is 0.11°, which corresponds to about 12.5 km. Prein et al. (2016) shows that there is a benefit in using the 0.11° resolution over the 0.44° resolution when modeling precipitation, both for mean and extreme values. With the historical runs ranging untill 2006, the historical reference period was chosen to be 1971 to 2000. For the projection periods, a near future time range from 2021-2050 (NF) and distant future time range from 2071-2100 (DF) is defined. In general, a bigger model ensemble increases the robustness of the results. To further compare characteristics of the RCMs and GCMs, the biggest possible model ensemble where every RCM is nested in every GCM is chosen. Applying these criteria produces a model ensemble with 5 GCMs and 5 RCMs, resulting in 25 ensemble members. Fig. 3.1 shows the selected models.

Global climate models	Regional climate models
CNRM-CM5	COSMO-CLM
EC-EARTH	REMO
HadGEM2-ES	HIRHAM
MPI-ESM-LR	RACMO
NorESM1-M	RCA4

Figure 3.1: Global climate models (GCM) and regional climate models (RCM) of EURO-CORDEX regional climate simulations selected for the model ensemble. Every RCM is run with every GCM. Resolution is 0.11° and simulations are run under the RCP8.5 scenario.

The agreement of ensemble members is used to determine significance for trends in chapter 4. Jacob et al. (2014) uses a significance treshold of 66 % for the agreement of ensemble members in the sign of a trend. Implementing this method for the selected model ensemble means that a trend is significant if 17 of the 25 members (which is 68 %) agree in the sign of the trend.

3.2 E-OBS

The ENSEMBLES daily gridded observational data set for precipitation, temperature and sea level pressure in in Europe (E-OBS) is a data set of interpolated station data (Cornes et al., 2018). Here, the ensemble mean of version E-OBS V20e is used. It is chosen because it is available on a similar grid size (0.10°), provides daily precipitation values on climatological time scales and covers the observation area, as it contains all of the European land surface. The precipitation data set is generated by interpolating station data from approximately 9000 stations. The method of interpolation and ensemble generation is described in (Cornes et al., 2018). It should be noted that the station density is quite inhomogeneous and is decreasing in the South of the domain and that uncertainty in the data set is strongly depending on station coverage (Cornes et al., 2018). In general, interpolated observational data sets have uncertainties and are not a representation of reality (Hofstra et al., 2009). Assessing and adjusting model data with E-OBS therefore inherits this uncertainty. However, E-OBS is a commonly used data set for evaluating regional climate modeling output (Herrera et al., 2016). Furthermore, Cardell et al. (2019) used E-OBS as reference data for bias adjustment of regional climate modeling data.
The Iberia01 data set (Herrera et al., 2019) would be an alternative to E-OBS. However, the bias correction method was applied for the whole EURO-CORDEX domain and Iberia01 covers only the IP. The Tropical Rainfall Measuring Mission data set (TRMM) (Huffman et al., 2007) offers direct observation data instead of interpolated station data and could be useful for evaluating model output. However, there is a mismatch in available time periods and the uncertainty in TRMM data is increasing with latitude.

3.3 Bias correction

Systematic biases in climate models are common and can be caused for example by insufficient representation of physical processes (Liang et al., 2008). Fig. 3.2) shows that model data has substantial biases in rainfall amounts and big deviations amongst ensemble members for the reference period. However, realistic precipitation values and comparability of ensemble members are desirable. Therefore, a bias correction method is applied.
Yang et al. (2018) proposes a bias correction method for projection data that aims at conserving changes in frequency distributions of precipitation. It is using a transfer function that incorporates cumulative density functions of fitted gamma distributions. However, results of this method did not seem promising. Possible reasons are, that the number of precipitation events at some points and months is too low and that the treshold for minimum precipitation amounts in E-OBS is too high to allow a good fit of gamma functions. The quantile-quantile adjustment method used in Cardell et al. (2019) is using transfer functions for quantiles without fitting gamma distributions. This method is able to transfer the climate change signal in mean, variance and extremes of the

distribution, and should therefore produce useful results. However an implementation is not further pursued due to the time restraints of this thesis. Instead, a 'simple multiplicative correction of precipitation' (Berg et al., 2012) is chosen, which is adjusting precipitation values by using monthly means.

Before the actual bias correction is applied, all precipitation values below 0.1 mm/day are removed, as they are not believed to be physically meaningful (drizzle correction). In a first step, climatological monthly precipitation sums during the reference period are calculated for the observational and model data. The ratio of those sums serves as correction factor. Every model precipitation value is then scaled with this factor for the respective model, month and grid point. Because under certain conditions this ratio can reach big values, the correction factor is set to 0.02 when below 0.02, and to 50 if above 50.

$$pr^i_{BC}(t) = pr^i_{mod}(t) \cdot \frac{\overline{\Sigma pr^i_{obs}(mon)}}{\overline{\Sigma pr^i_{mod}(mon)}} \tag{3.1}$$

With the bias corrected precipitation value $pr^i_{BC}(t)$, the corresponding raw model value $pr^i_{mod}(t)$, the climatological monthly sum of the observational data $\overline{\Sigma pr^i_{obs}(mon)}$ and the climatological monthly sum of the model data $\overline{\Sigma pr^i_{mod}(mon)}$.

The underlying assumption is that the relationship of real world precipitation and model precipitation does not change under future climate conditions.

3.4 Evaluation

Fig. 3.2) presents a first overview of precipitation in models compared to E-OBS. Shading displays the ratio of annual rainfall sums of reference data to ensemble mean in the reference period (1971-2000). Models mostly overestimate precipitation, as the ratio is well below 1 in large parts of the IP. The South West IP is the only region where E-OBS exceeds the ensemble mean. Values are between 0.5 and 1 in most parts of the IP. This rainfall ratio also indicates the spatial pattern of the correction factor. However, these values are averaged over 25 ensemble members and summed up over 12 months. The ratio for single models and months can be substantially smaller or bigger. In these cases, the correction method acts deflating or inflating for the precipitation changes of the raw model data. The standard deviation of climatological annual rainfall among ensemble members is depicted by the contour lines in Fig. 3.2, which have intervals of 500 *mm*. The biggest standard deviations are in mountain regions and at the coastal regions in the North and West, which is not surprising, since precipitation is also biggest in these regions. In these areas, the standard deviation exceeds 500 *mm* and reaches up to 1500 *mm* at some grid points. These are substantial deviations, as this about the magnitude of annual precipitation in Fig. 2.1 at these locations.

Fig. 3.3 a) illustrates the effect of the bias correction on the climatology of model data with an example. The grid point is in central Spain, near Madrid. The data is from the model run with CNRM-CM5 as GCM and COSMO-CLM as RCM. The bias correction removes the difference between model and E-OBS run for the reference period, which is not surprising, as it is defined to do so. In the process of bias correction, the ratio of precipitation in reference period and projection model runs is conserved in sign and scaled with the correction factor.

The frequency distribution of precipitation in January for the same data sets and the same grid point is shown in Fig. Fig. 3.3 b). The curves show the cumulative density function of fitted gamma functions of the corresponding distributions. The curves of raw model data have higher extreme intensities than E-OBS. However, they also have a stronger incline at low precipitation values. Even though the bias correction does not correct the shape of the distribution, the scaling is reducing the difference between E-OBS and model data. While the distributions differ a lot between grid points, it seems as though very high precipitation values remain in the bias corrected data. Subsequently, drought indices have a higher dependence on single rainfall events and could therefore be influenced in their reliability.

In general, the models seem to overestimate precipitation, in some locations quite severely. The bias correction method successfully adjusts climatological precipitation sums. Locally, the correction factor can reach extreme small and big values, which under specific circumstances could disturb the climate signal. However, no numerical artifacts could be detected that would substantially influence the results. Even though the BC is not aiming at adjusting the distribution, it decreases the difference to the E-OBS distribution in most cases. The bias correction method therefore should be sufficient in assessing the research questions.

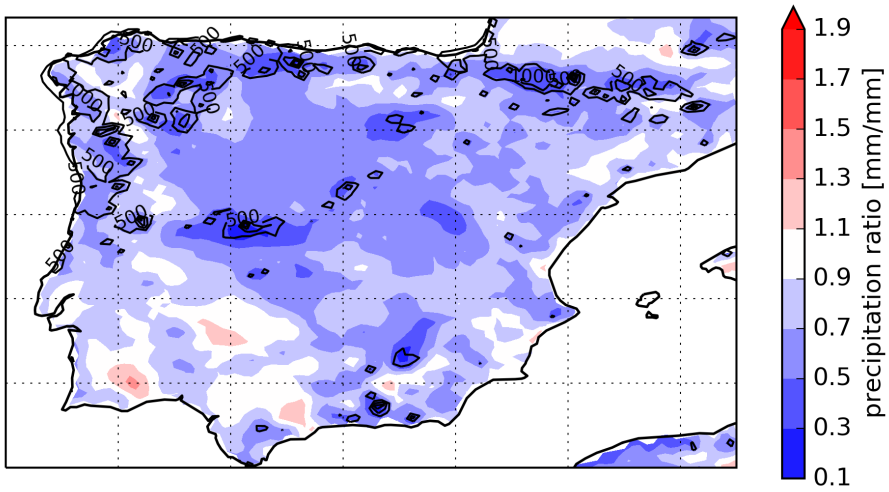

Figure 3.2: Ratio of annual mean precipitation between E-OBS V20e and the model ensemble mean (shaded) and standard deviation among ensemble members (black lines, contour interval is 500 *mm*) for the reference period (1971-2000).

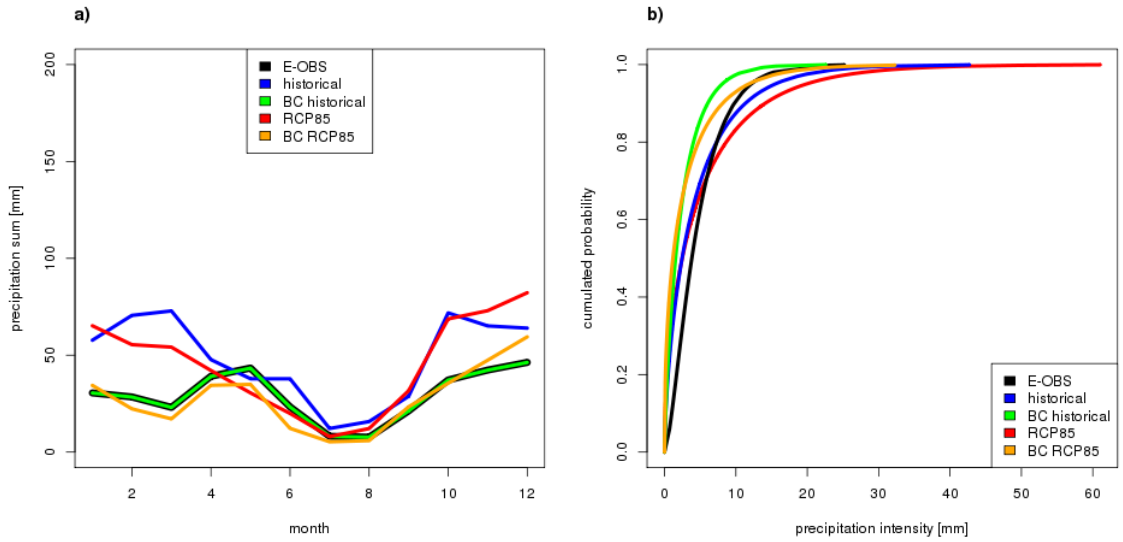

Figure 3.3: a) Climatological monthly precipitation (in *mm*) at a grid point near Madrid (40.09°N, 4.29°W). Data from E-OBS V20e (1971-2000, black line), the uncorrected model ensemble in the reference period (1971-2000, blue line), the bias corrected model ensemble in the reference period (1971-2000, green line), the uncorrected model ensemble in the projection period (2006-2100, red line) and the bias corrected model ensemble in the projection period (2006-2100, orange line). b) Fitted Cumulative Density Function of daily precipitation (in *mm*) distribution for the month of january at the same grid point as in a). Data from E-OBS V20e (1971-2000, black line) and a single model run (CNRM-CM5-COSMO-CLM) with the uncorrected model run in the reference period (1971-2000, blue line), the bias corrected model run in the reference period (1971-2000, green line), the uncorrected model run in the projection period (2006-2100, red line) and the bias corrected model run in the projection period (2006-2100, orange line).

4 Results

This chapter is targeting to answer the research questions formulated in chapter 1. To do so, several aspects of RDs in a changing climate are addressed in the following sections. Section 4.1 is analyzing the changes in precipitation in the annual cycle. Section 4.2 investigates changes in temporal mean and variability of the Effective Drought Index (EDI). In section 4.3, the changes in (maximum) duration of RDs are examined, while 4.4 is studying the changes in RD frequency. The areas used for the analysis of the IP and its subregions are defined in Fig. 2.1. The criterion for significance, adopted from Jacob et al. (2014), is described in section 3.1.

4.1 Precipitation changes

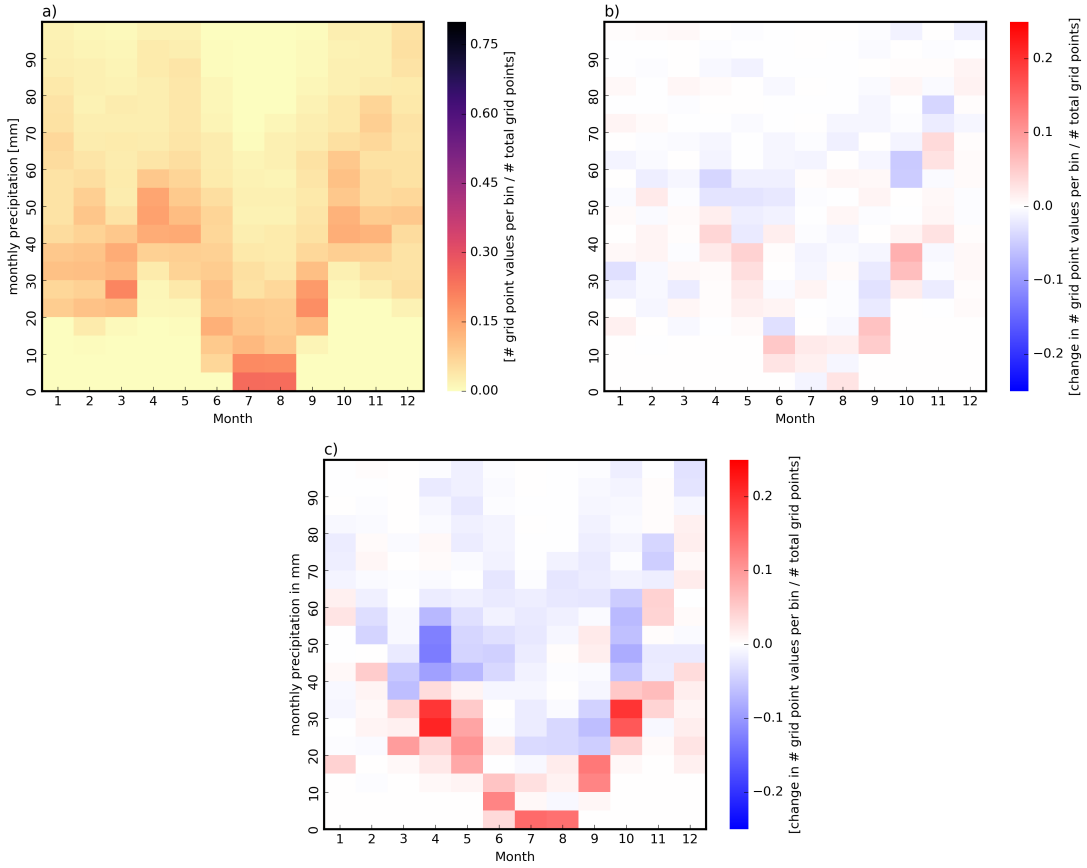

Figure 4.1: Distribution of the ensemble mean of climatological monthly precipitation sums (in *mm*) in the IP (36°N to 44°N, 10°W to 3°E). Shading indicates the ratio between the number of grid point values per bin and the number of total grid points. a) shows the absolute ratio for the reference period (1971-2000), b) shows the difference between the NF (2021-2050) and the reference period, c) shows the difference between the DF (2071-2100) and the reference period.

This section provides an overview of the projected climatological precipitation changes of the ensemble mean over the course of the annual cycle.
In a first qualitative assessment, Fig. 4.1 shows monthly climatological values of the ensemble mean over the annual cycle for every grid point in the IP. The shading indicates the ratio of number of grid point values in an precipitation interval divided by the total number of grid points in the IP. Fig. 4.1 a) shows the absolute values of this ratio for the reference period. Fig. 4.1 b) and 4.1 c) represent the changes in this ratio with regard to the reference period for the NF and DF. This illustrates the annual cycle and the spatial inhomogeinity of precipitation and the projected changes. In Fig. 4.1 a), the distribution of precipitation across the IP has a big spread in November, December and January and shows bimodal characteristics. The distribution is more homogeneous in spring and autumn. In the months of July and August, values are mostly confined to bins below 25 *mm*. The distribution is shifted towards lower values for the future periods. Overall, more smaller values and less higher values are projected in the NF (Fig. 4.1 b)). Between April and October, the signal is quite clear, however, it is rather diffuse in the winter months. For the DF, we see that the pattern becomes clearer and intensifies. The drying signal can be identified for every part of the annual cycle, with the strongest changes in April and October Also, the trend is more pronounced towards the southern regions (not shown).
The climatological monthly precipitation values of the ensemble mean suggest a shift towards less rainfall. The signal is stronger in the DF than in the NF and especially strong in spring and autumn.

4.2 General drought statistics

This section assesses the trend in general drought conditions by decomposing it to changes in temporal mean and variability of the Effective Drought Index (EDI). For both properties, the spatial pattern of the ensemble mean is explored. Differences across ensemble members are examined by comparing spatial means of the IP, and for the temporal mean of EDI also for the IP-SE and Fig. B regions. For the reference period, the temporal mean of EDI is 0 and the temporal standard deviation is 1 per definition (section 2.2.4). Therefore, only the NF and DF, but not the reference period are analyzed. Temporal mean values below (above) 0 indicate a drying (wettening), and temporal variability values below (above) 1 indicate lower (higher) temporal variability with regard to the reference period. In the following text, it is implied that EDI values have the unit of 'standard deviation'. For example, an EDI value of -1 means that Effective Precipitation (EP) is reduced by 1 standard deviation of the climatological distribution of the reference period.

Changes in the ensemble mean of temporal mean of EDI are first addressed to identify a possible tendency towards dryer conditions in climate projections.
Fig. 4.2 displays these changes for the NF and DF. In Fig. 4.2 a), there is a drying trend for most of the IP in the NF. The mountain ranges and large parts of Portugal show a stronger trend than the rest of the IP with EDI values below -0.4. Interestingly, some areas along the eastern coast exhibit a slightly positive trend in EDI. In Fig. 4.2 b), the drying signal is prevailing in all of the IP. Values are between -0.4 and -0.6 in most parts of the IP. The most extreme values are below -1.0. In the DF, the pattern of the strongest drying trends has changed slightly, as values in the central mountain ranges decreased stronger than in Portugal. When interpreting the values in Fig. 4.2,

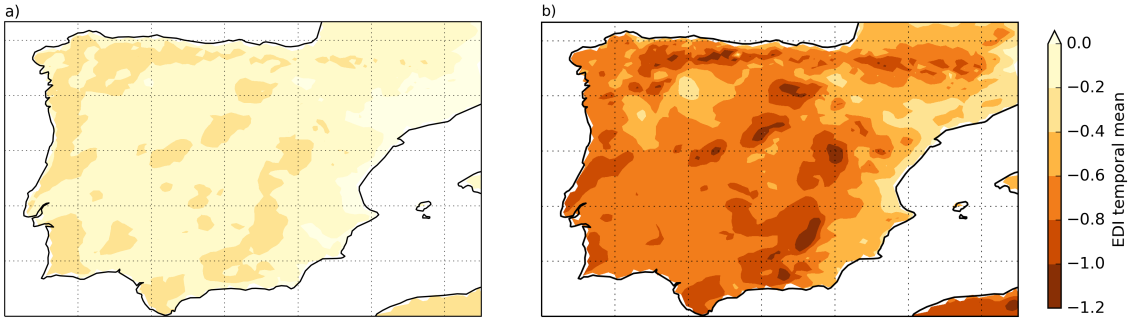

Figure 4.2: Effective Drought Index (EDI), ensemble mean of temporal mean, a) for the NF (2021-2050) and b) for the DF (2071-2100).

one has to keep in mind that these are the values of the ensemble mean. Single runs may differ in the strength of the drying trend and also in the spatial patterns. Also the field gets smoothed by averaging over the model ensemble.

Overall, a clear shift of mean conditions towards drought in the IP over the course of the century is indicated. The trend is significant in large areas of the IP in the NF (Appendix, Fig. B.5 a)) and in all areas of the IP in the DF (Appendix, Fig. B.5 b)).

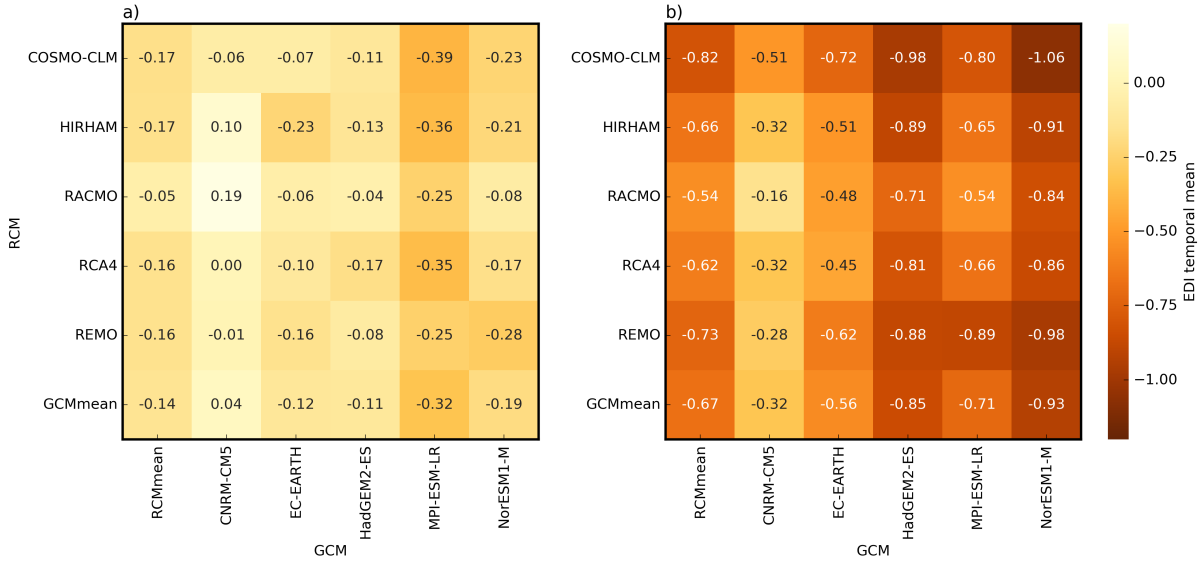

Figure 4.3: Effective Drought Index (EDI), spatial mean over the IP (36°N to 44°N, 10°W to 3°E) of temporal mean a) for the NF (2021-2050) and b) for the DF (2071-2100). Every box represents the value of an ensemble member. The corresponding GCM (RCM) to a model run is listed below the bottom row (left of the leftmost column). The bottom row (leftmost column) depicts the model mean value of all ensemble members with that GCM (RCM). The bottom left value is the ensemble mean.

The strength of the drying signal among the single ensemble members is assessed in the following. The variability of the climate mean signal in EDI across ensemble members is shown in Fig. 4.3. The values in the boxes represent the temporally and spatially averaged field of EDI for the respective time period and combination of RCM and GCM. RCMs are aligned in rows and GCMs in columns. Additionally, the leftmost column and the bottom row show the mean values of the RCMs and GCMs over the respective ensemble members. To analyze the influence of different

GCMs and RCMs, the following findings mainly describe these means. The ensemble average is on the bottom left. The shading of the box resembles its EDI value. Overall, the shift towards dryer conditions in the NF is confirmed in Fig. 4.3 a). 22 of 25 ensemble members project a drying trend. CNRM-CM5 is the only GCM that shows a positive trend and is the driving GCM of all 3 ensemble members with non-negative values. MPI-ESM-LR on the opposite has the strongest drying signal of all GCMs. For the RCMs, RACMO has the weakest drying trend while the other RCMs have a similar magnitude in the strength of the climate change signal. Fig. 4.3 b) indicates a stronger drying for the DF, with an overall average value of -0.67. For the DF, there is consentaneous agreement in the sign of change across ensemble members, but with a spread of about an order of magnitude (-0.16 and -1.06). While CNRM-CM5 is also the least drying GCM in DF, NorESM1-M has, unlike the NF, the strongest drying signal. RACMO is again the RCM with the smallest change, COSMO-CLM has the biggest change. Most ensemble members suggest a strong acceleration in the drying trend towards the end of the 21st century, with the exception of the MPI-ESM-LR driven runs, that have a more steady decrease in EDI.

For the NF, there is wide agreement and for the DF absolute agreement in the sign of temporal and spatial mean EDI trend and therefore trends are significant for both periods. However, the variability in magnitude of change is quite big among the ensemble members. GCMs display a stronger influence than RCMs on the strength of the climate signal in single ensemble members. This appears logical, as precipitation in the IP is highly depending on the large scale flow, which is mostly determined by the driving GCM.

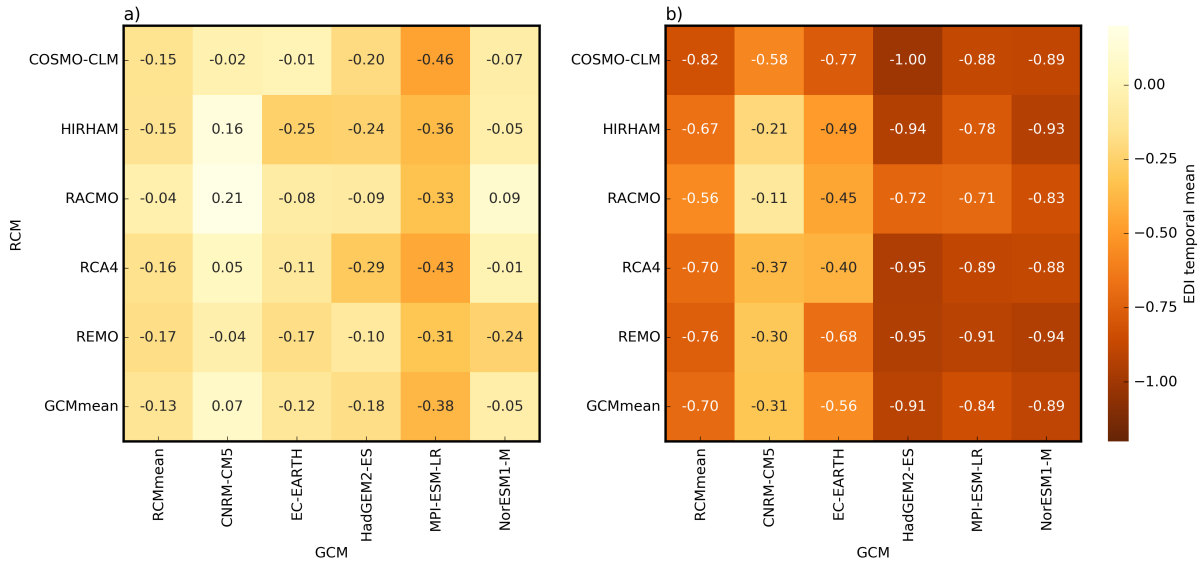

Figure 4.4: same as Fig. 4.3, but for IP-SE (36°N to 40°N, 5°W to 0°E).

The different regional patterns among ensemble members in temporal mean spatial mean EDI are addressed in detail for the IP-SE and IP-SW region.

Fig. 4.4 and Fig. 4.5 are the same as Fig. 4.3, but for the IP-SE and IP-SW region respectively. In the NF, ensemble means in both regions are negative, with -0.13 in the IP-SE (Fig. 4.4 a)) and -0.18 in the IP-SW (Fig. 4.5 a)). Interestingly, ensemble members display a different spatial focus of drying. Among GCMs, EC-EARTH and NorESM1-M have a more negative value in

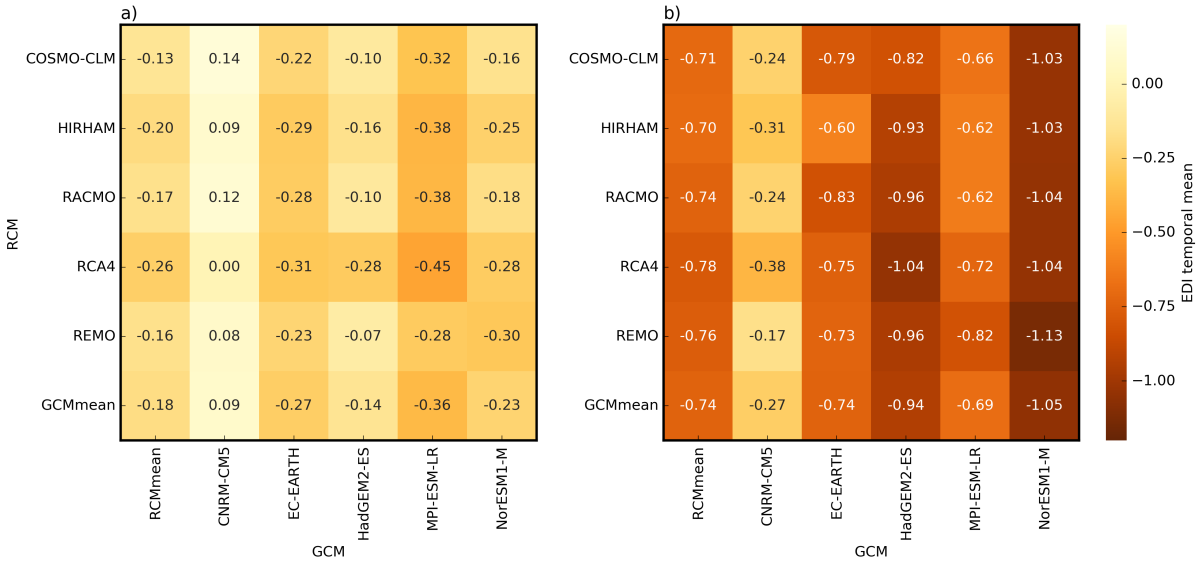

Figure 4.5: same as Fig. 4.3, but for IP-SW (36°N to 40°N, 10°W to 5°W).

the IP-SW. The other GCMs project a stronger drying in the IP-SE, but with a smaller margin between the two regions. Such regional differences are also existent among RCMs, even though they are smaller. RCA4, RACMO and HIRHAM project a stronger drying in the IP-SW, the other two RCMs project slightly dryer conditions for the IP-SE. In the DF (Fig. 4.4 b) and Fig. 4.5 b)), the ensemble mean values of the two regions are again close (-0.70 in the IP-SE and -0.74 in the IP-SW). Comparing GCMs, the IP-SW has a bigger change than IP-SE in temporal mean spatial mean EDI with EC-EARTH and NorESM1-M, while it is the other way round with MPI-ESM-LR. Among RCMs, both RACMO and RCA4 have a stronger drying signal in the IP-SW than in the IP-SE. COSMO-CLM on the other hand produces stronger drying trends in the IP-SE.

Also in the IP-SE and IP-SW regions, trends in temporal mean spatial mean EDI are negative and significant. The ensemble mean values are similar, but there is a striking variability in regional drying patterns among ensemble members. Depending on both GCMs and RCMs, a stronger drying signal can be identified rather in the eastern or the western regions. This could be connected to different responses of the circulation to climate change. The tables of temporal mean spatial EDI for the other subregions are in the Appendix (Fig. B.2, B.3 and B.4).

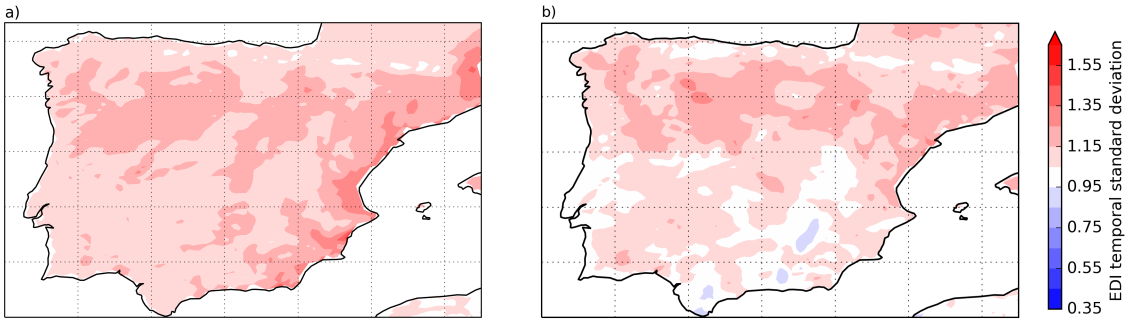

Figure 4.6: Effective Drought Index (EDI), ensemble mean of temporal standard deviation a) for the NF (2021-2050) and b) for the DF (2071-2100).

Next, the changes in the temporal variability of EDI are investigated, to complement the picture of general drought properties in the model runs.

Similar to Fig. 4.2, the ensemble mean of the temporal standard deviation of EDI is displayed in Fig. 4.6. Fig. 4.6 a) shows a trend towards higher temporal variability in the NF. Almost all parts have values over 1.05 and large parts also over 1.15. Areas of high increase in variability are in the northern inland and along the Mediterranean coast. In the DF, the difference in temporal variability between North and South becomes bigger (Fig. 4.6 b)). While values remain above 1.15 in most parts, bigger areas in the South have values below 1.05 and some even below 0.95. This turn in temporal variability trend in the South could be a consequence of a drying trend in areas that are already relatively dry in the reference period. An additional drying can only be caused by very low precipitation values over a long period, which decreases temporal variability.

The overall picture suggests higher temporal variability in EDI in the NF (significant increase in almost all locations, Appendix, Fig. B.6 a)). In the DF, increases compared to the reference period are significant in the North and some parts of the South (Appendix, Fig. B.6 b)). Overall, the increase is more prominent in the northern parts of the IP.

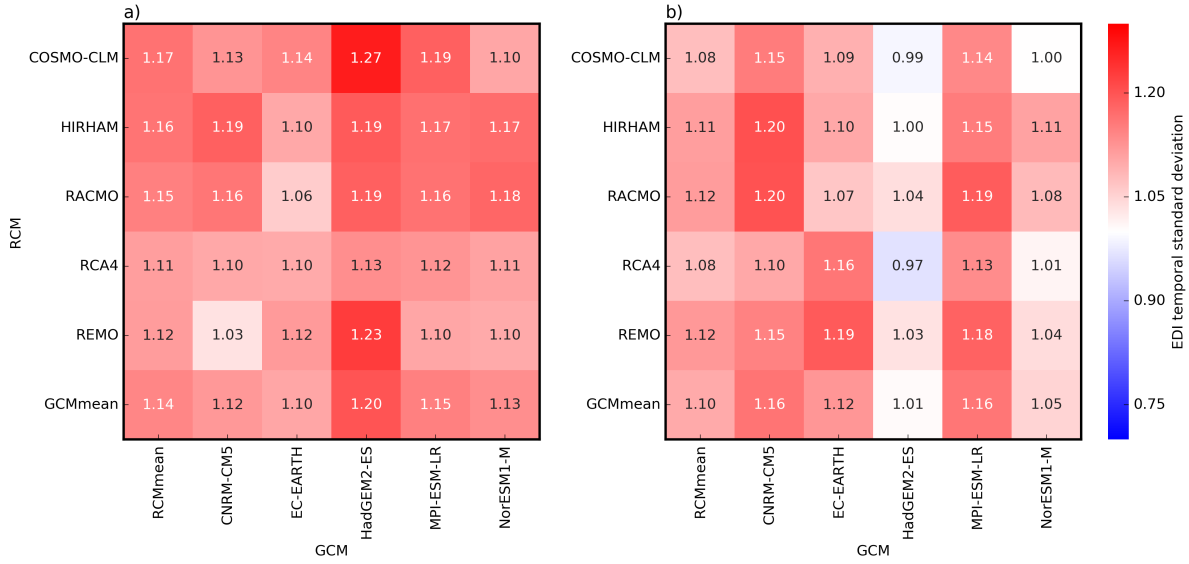

Figure 4.7: Effective Drought Index (EDI), spatial mean over the IP of temporal standard deviation a) for the NF (2021-2050) and b) for the DF (2071-2100). The table is structured like Fig. 4.3.

The differences in the temporal EDI variability trend among ensemble members are addressed to deepen the understanding of possible drought changes in the model ensemble under climate change.

The temporal standard deviation of EDI of the respective ensemble member and time period is spatially averaged and displayed in Fig. 4.7, which is structured the same way as Fig. 4.3. Fig. 4.7 a) shows that there is absolute agreement among model members in an increase in temporal variability in the NF. In the DF, the picture is less uniform (Fig. 4.7 b)). The ensemble mean is 1.10, which is smaller than in the NF. The spread becomes bigger, with values between 0.97 and 1.20. The models with HadGEM2-ES and NorESM1-M as GCM decrease in temporal variability and

are now closer to 1 or even below. These ensemble members show the strongest drying signal in Fig. 4.3 b), which further supports the hypothesis that a strong drying signal decreases variability. In EDI, there is a general trend towards higher temporal variability in the NF. The trend turns around for some members in the DF. Variability among ensemble members seems to be driven by GCMs rather than RCMS, especially when the GCM forces a very strong drying signal that decreases variability.

The results in this section display a trend towards dryer conditions in the temporal mean and higher temporal variability of EDI. This increases the probability of drought occurrence and subsequently also the probability of RD.

4.3 Recurrent drought duration

In this section, the changes in maximum RD duration under future climate conditions will be examined. To provide a robust picture, this is done by using four different indices: The Recurrent Dry Year Index (RDYI), the Consecutive Drought Year Index based on EDI at single Grid Points (CDY_EDI_GP), the Consecutive Drought Year Index (CDY) and the Consecutive Drought Year Index based on EDI (CDY_EDI). RDYI and CDY use relative deviations of annual precipitation sums to identify dry/drought years, CDY_EDI_GP and CDY_EDI use EDI. RDYI and CDY_EDI_GP produce two dimensional fields, so the ensemble mean is used to identify spatial patterns of maximum RD duration. CDY and CDY_EDI poduce one dimensional digits and are used for a comparison of ensemble members. The indices are applied for reference period, NF and DF. All numerical values of these indices have the time unit 'year'. For example, a CDY of 5 means that the longest streak of drought years is 5 years long.

To assess the spatial patterns of the maximum duration of dry periods, the ensemble mean of RDYI is investigated for the reference period, NF and DF.
For the reference period, the ensemble mean is below 2 at all locations, RDs in the model ensemble therefore should be rare in this period (Fig. 4.8 a)). In the NF (Fig. 4.8 b)), only the southernmost part of the IP has values above 2, while some locations in the North are below 1. However, Fig. 4.8 c) indicates an increase in the maximum duration of dry periods in the DF, with an RDYI of at least 2 in all locations and an increase towards the South, where large areas show 4 and some hotspots in the Baetic System even 6. Single ensemble members may exhibit varying spatial patterns, similar to the regional changes in EDI trends in Fig. 4.4 and 4.5.
The climate change signal in RDYI is more pronounced in the South than in the North. There is only a clear increase in RDYI in the DF (significant in large areas towards the South, Appendix, Fig. B.7 b)), as in most locations the ensemble mean of the RDYI is not sensible enough to detect changes in the NF (significant in some parts of the South, Appendix, Fig. B.7 a)).

To explore the pattern of changes in maximum duration of RDs with an EDI based drought definition, the ensemble mean of CDY_EDI_GP is investigated.
Fig. 4.9 a) shows that in the reference period, the ensemble mean exceeds a value of 2 in large parts of the North. In the NF (Fig. 4.9 b)), the field is remarkably uniform, with most grid points

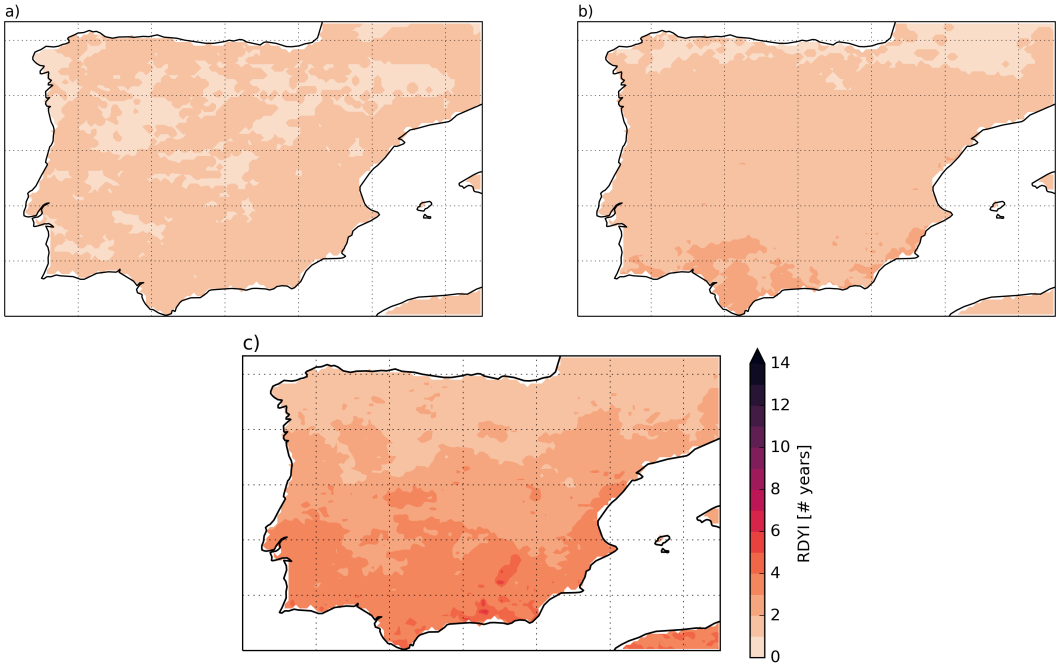

Figure 4.8: Recurrent Dry Year Index (RDYI), ensemble mean a) for the reference period (1971-2000), b) for the NF (2021-2050), c) for the DF (2071-2100).

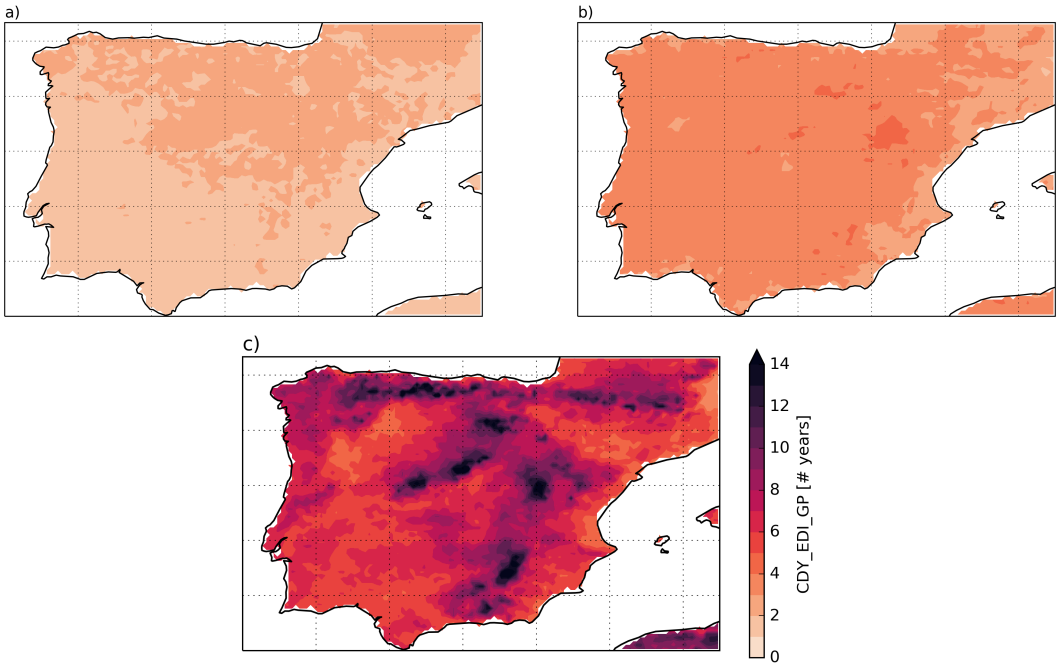

Figure 4.9: Consecutive Drought Year Index based on EDI at single Grid Points (CDY_EDI_GP), ensemble mean a) for the reference period (1971-2000), b) for the NF (2021-2050) and c) for the DF (2071-2100).

at values between 3 and 4. Single locations are above or below this interval. For the DF, the ensemble mean increases further (Fig. 4.9 c)). The pattern roughly reshapes elevation, with higher values in higher elevations. The biggest values of over 15 are found in the mountain ranges (in this order of magnitude, the maximum RD duration is mainly determined by the position of the

non drought year in the time series). The lowest values are below 5 in the Douro and Ebro basins and some locations along the eastern coast.

Overall, the CDY_EDI_GP ensemble mean shows a strong increase in maximum RD duration. CDY_EDI_GP generally detects longer RDs than RDYI and the increase in RD duration is significant in larger areas (Appendix, Fig. B.8). Elevation seems to be the most important geographical feature for changes in CDY_EDI_GP, whereas in RDYI, latitude was the prevailing factor. This is because the temporal variability of annual precipitation sums relative to climatological annual precipitation sums in the reference period is bigger in the South than in North and decreased in mountain ranges (Appendix, Fig. B.1). Areas with high interannual precipitation variability have a relatively low sensitivity for the EDI based drought definition, because EDI is standardized with temporal variability. Areas with low interannual variability have a relatively low sensitivity for the relative annual precipitation based drought definition.

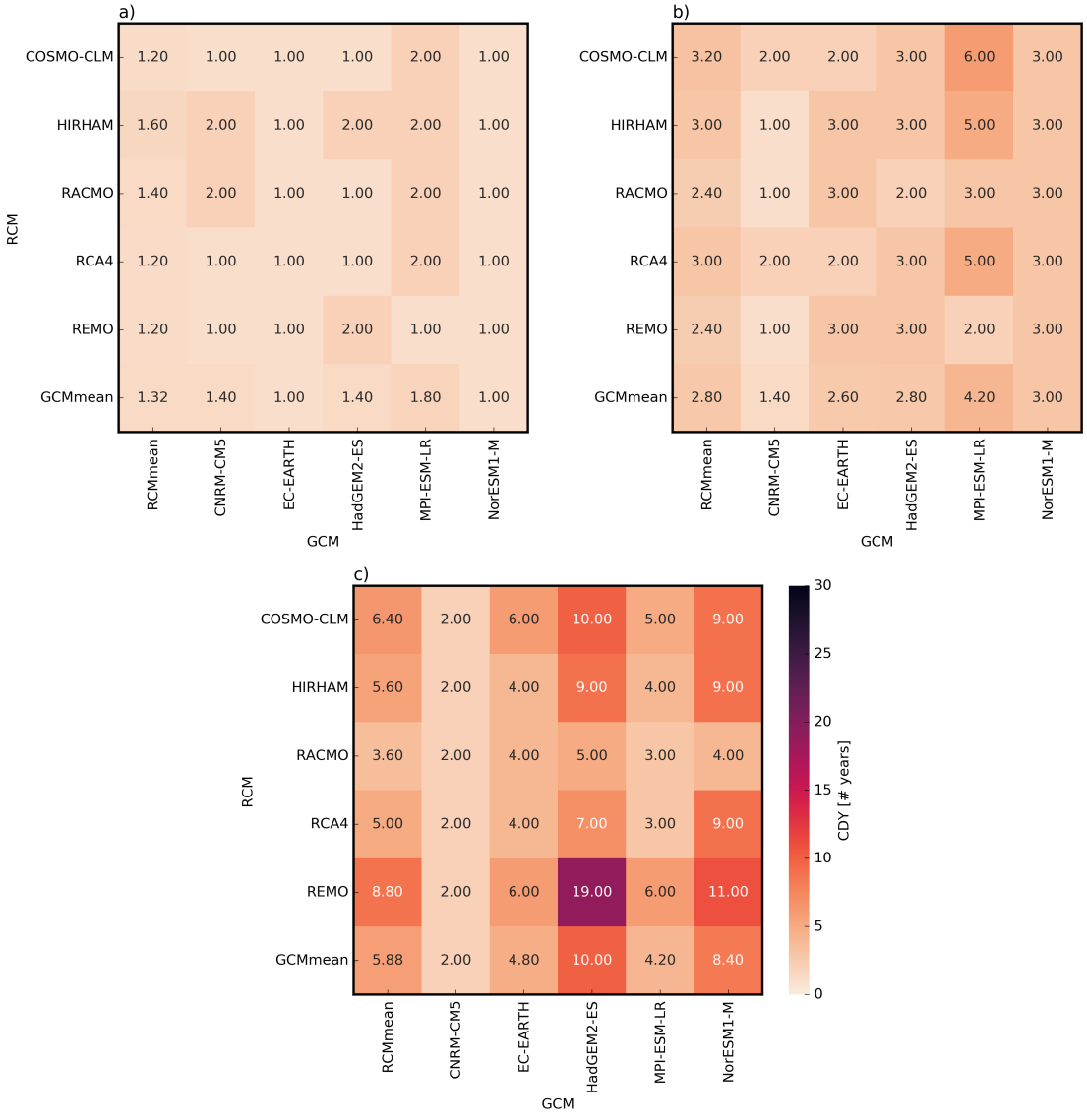

Figure 4.10: Consecutive Drought Year Index (CDY) in the IP a) for the reference period (1971-2000), b) for the NF (2021-2050) and c) for the DF (2071-2100). The table is structured like Fig. 4.3.

The CDY is used to address the change in maximum drought duration in the IP and detect differences across ensemble members for this value. Model mean values are described mostly to analyze the influence of models on single ensemble members.

Fig. 4.10 shows the CDY for the IP and is structured like Fig. 4.3. The overall average value for the reference period is 1.32 (Fig. 4.10 a)). All members have a CDY of either 1 or 2. Four of five runs with MPI-ESM-LR detect a RD, while EC-EARTH and NorESM1-M have no ensemble members with a CDY of 2. In Fig. 4.10 b), the ensemble mean increases to 2.8 for the NF. Almost all ensemble members are increasing in CDY, with a maximum value of 6. However, two members decrease to 1. The three members that have the lowest values are all driven with CNRM-CM5 as GCM, while members with MPI-ESM-LR as GCM have the highest values. This is consistent with the previous analysis of mean climate trends among ensemble members and especially the characteristics of GCMs (Fig. 4.3 b)). While an overall increase in CDY is suggested, not all ensemble members agree on the sign of the trend. For the DF, the overall change rises to 5.88 years (Fig. 4.10 c)). The spread is quite big with values between 2 and 19 years. The CNRM-CM5 driven ensemble members all remain at 2, the HadGEM2-ES and NorESM1-M driven runs show a strong increase. Again, the picture is consistent with the changes found in temporal mean of EDI (Fig. 4.3 c)).

The CDY suggests an increase in maximum drought duration with significant trends for both the NF and DF. The signal is stronger for the DF. The variation across models is big, as some show no increase. Others project drastic increases that suggest permanent drought conditions in the DF. The GCMs have a higher influence on ensemble variability and the model characteristics are similar to those found for the spatial mean temporal mean change of EDI.

The maximum RD duration and the differences across ensemble members are investigated with the CDY_EDI in a similar way to the CDY before.

Fig. 4.11 is structured like Fig. 4.3. In the reference period, the ensemble mean is 1.56, with values ranging from 1 to 3 (Fig. 4.11 a)). For the NF, the ensemble mean rises to 3.56, with values between 1 and 6 (Fig. 4.11 b)). Two ensemble members, both driven with the CNRM-CM5 GCM, show a decrease in CDY_EDI. Three more members remain at the same values, two of them driven with CNRM-CM5 and one driven with MPI-ESM-LR, which is surprising, as the model mean for MPI-ESM-LR has the strongest increase in the NF. In the DF, the ensemble mean of CDY_EDI increases to 9.6. The minimum value is only 3, while the maximum is 29. HadGEM2-ES driven runs produce by far the biggest increases in maximum RD duration. CNRM-CM5 runs again have the smallest changes.

In CDY_EDI, an increase in maximum drought duration is projected. Models agree on sign in most cases for the NF and all cases for the DF (significant). The magnitude of change is strongly varying between ensemble members, reaching from only slight increases to the duration of the whole period, projecting an permanent state of drought. CDY_EDI detects longer RDs and also stronger increases in maximum RD duration than CDY. The spread among GCMs is slightly bigger than that of RCMs. The influence on the CDY_EDI of the ensemble members is therefore more balanced than for the CDY.

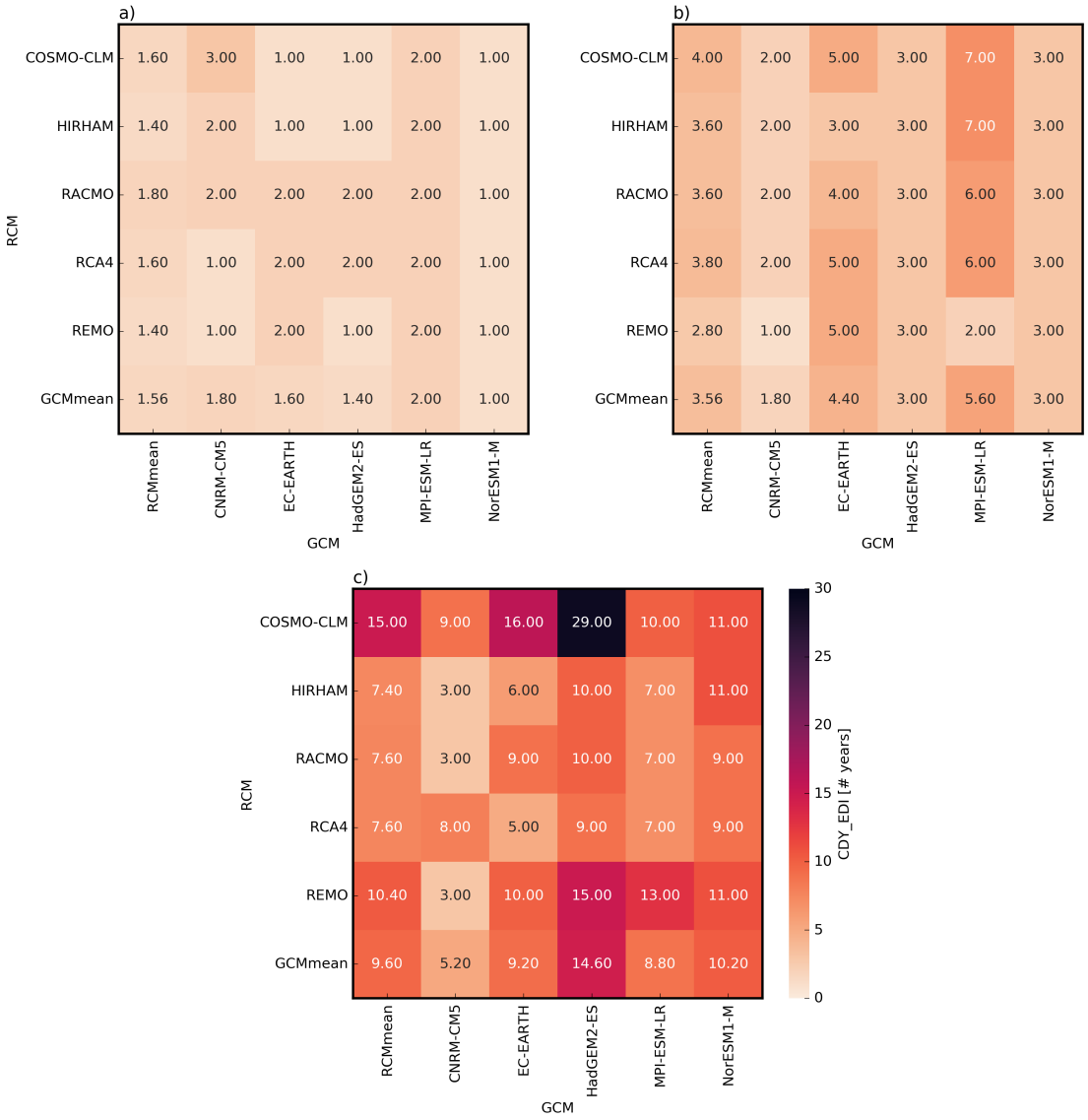

Figure 4.11: Consecutive Drought Year Index based on EDI (CDY_EDI) in the IP a) for the reference period (1971-2000), b) for the NF (2021-2050) and c) for the DF (2071-2100). The table is structured like Fig. 4.3.

Overall, the model ensemble projects an increase in maximum RD duration that is particularly strong in the DF. The trend is robust, as it is consistent among indices using drought year definitions based on relative annual precipitation and EDI. In general, the EDI based drought year definition proves to be more sensitive. Increased duration makes single RD events likely to have a bigger impact under future climate conditions.

4.4 Recurrent drought frequency

RD frequency is analyzed in the reference period, NF and DF. It is related to RD damage not only by the number of events but also by the regeneration time between events. Four different indices are used: The Number of Dry Periods (NDY), the Number of Drought Periods based on EDI at single Grid Points (NDP_EDI_GP), the Number of Drought Periods (NDP) and the Number of

Drought Periods based on EDI (NDP_EDI). Like in section 4.3, relative annual precipitation sums (for NDY and NDP) and EDI (for NDP_EDI_GP and NDP_EDI) are used to detect dry/drought years, which increases the robustness of the results. NDY and NDP_EDI_GP form two dimensional fields and spatial patterns of the ensemble mean are analyzed. NDP and NDP_EDI are one dimensional digits and are used to examine the variations across ensemble members. The unit of these indices is 'number of events per time period'. A NDP of 4 means that 4 consecutive drought years are detected in the respective time period.

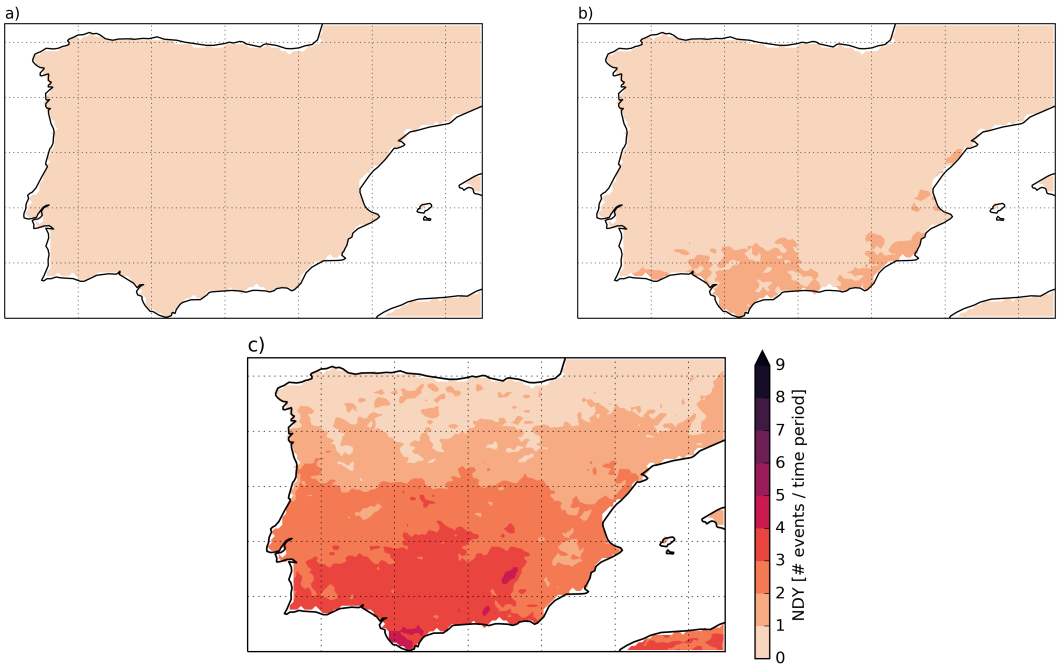

Figure 4.12: Number of Dry Periods (NDY), ensemble mean a) for the reference period (1971-2000), b) for the NF (2021-2050) and c) for the DF (2071-2100).

The ensemble mean of NDY is displayed to examine the spatial patterns in recurrent dry year frequency.

In Fig. 4.12 a), no location has a value above 1 in the reference period, which is consistent with Fig. 4.8 a). For the NF, Fig. 4.12 b) shows that ensemble mean NDY does exceed 1 only in the very South, consistent with Fig. 4.8 b). In Fig. 4.12 c), increasing values in NDY for the DF are shown, with a frequency of up to 3 RD events in the large parts of the South. The pattern again looks similar to the pattern of RDYI, it is however not identical. The big similarities in the spatial patterns of NDY and RDYI are because they use the same dry year definition.

The ensemble mean suggests an increase in the frequency of recurrent dry periods. The signal is increasing from North to South and rather weak for the NF. The pattern of model agreement and significance (Appendix, Fig. B.9) looks similar to that of the RDYI (Appendix, Fig. B.7).

The ensemble mean of NDP_EDI_GP is analyzed to obtain the pattern of RD frequency changes with an EDI based drought definition.

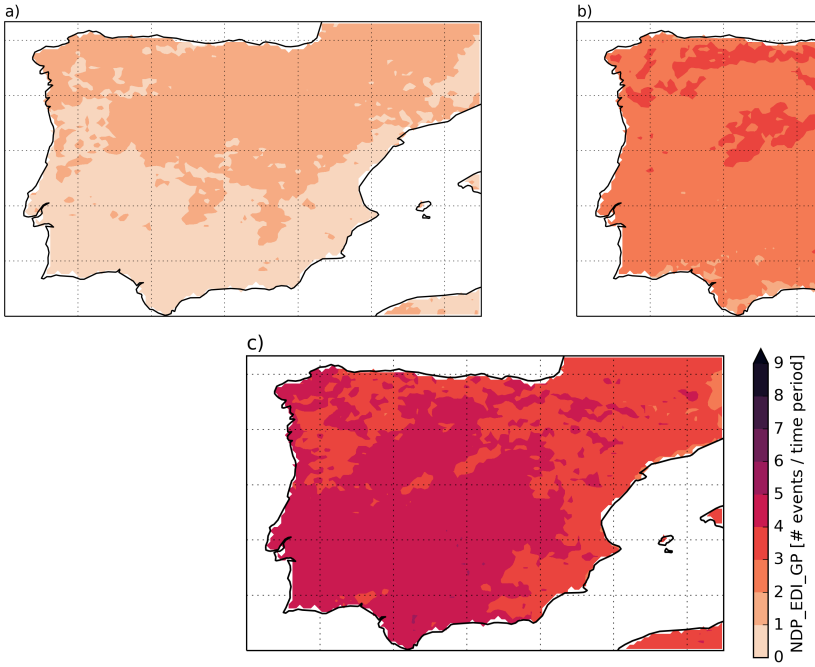

Figure 4.13: Number of Drought Periods based on EDI at single Grid Points (NDP_EDI_GP), ensemble mean a) for the reference period (1971-2000), b) for the NF (2021-2050) and c) for the DF (2071-2100).

In Fig. 4.13 a), the ensemble mean of NDP_EDI_GP exceeds 1 in parts of the North, consistent with the CDY_EDI_GP in Fig. 4.9 a). In the NF, most of the IP has values between 2 and 3. Values higher than 3 are mostly in mountainous areas, values below 2 are along the eastern and southern coast. In Fig. 4.13 c), values are between 4 and 5 towards the South West and most of the inland and between 3 and 4 in the rest of the IP. Single grid points in the South exceed 5. The Sistema Central has a prominent signature in the middle of the IP with lower values than its surrounding areas. Also in the other mountain ranges, a slightly smaller RD frequency change is projected. As those areas had the highest values of CDY_EDI_GP, this low frequency can be interpreted as a result of the very strong drying trend and a lack of non drought years.
Overall, NDP_EDI_GP suggest an increase in RD frequency, as does NDY. The increase is significant in most of the IP in the NF (Appendix, Fig. B.10 a)) and all of the IP in the DF (Appendix, Fig. B.10 b)). NDP_EDI_GP shows a more uniform field compared to NDY. The reason for these differences in spatial patterns are discussed in section 4.3.

The NDP counts RD events and is a one dimensional digit, it can therefore provide an overview of changes in RD frequency and the differences across ensemble members.
Fig. 4.14 shows values for the whole IP and is structured in analogous manner to Fig. 4.3. In Fig. 4.14 a), the ensemble mean is 0.33. All members have either 1 or 0 events in the reference period. For the NF, the ensemble average rises to 2.12 and frequency increases are projected for almost all members (Fig. 4.14 b)), again with the exception of the CNRM-CM5 driven runs, that show only a weak climate change signal in most tested indices. MPI-ESM-LR again has the highest increase among GCMs, but the pattern seems to be less pronounced than in other indices. The overall average reaches 3.92 in the DF, in Fig. 4.14 c). Most ensemble members indicate RD

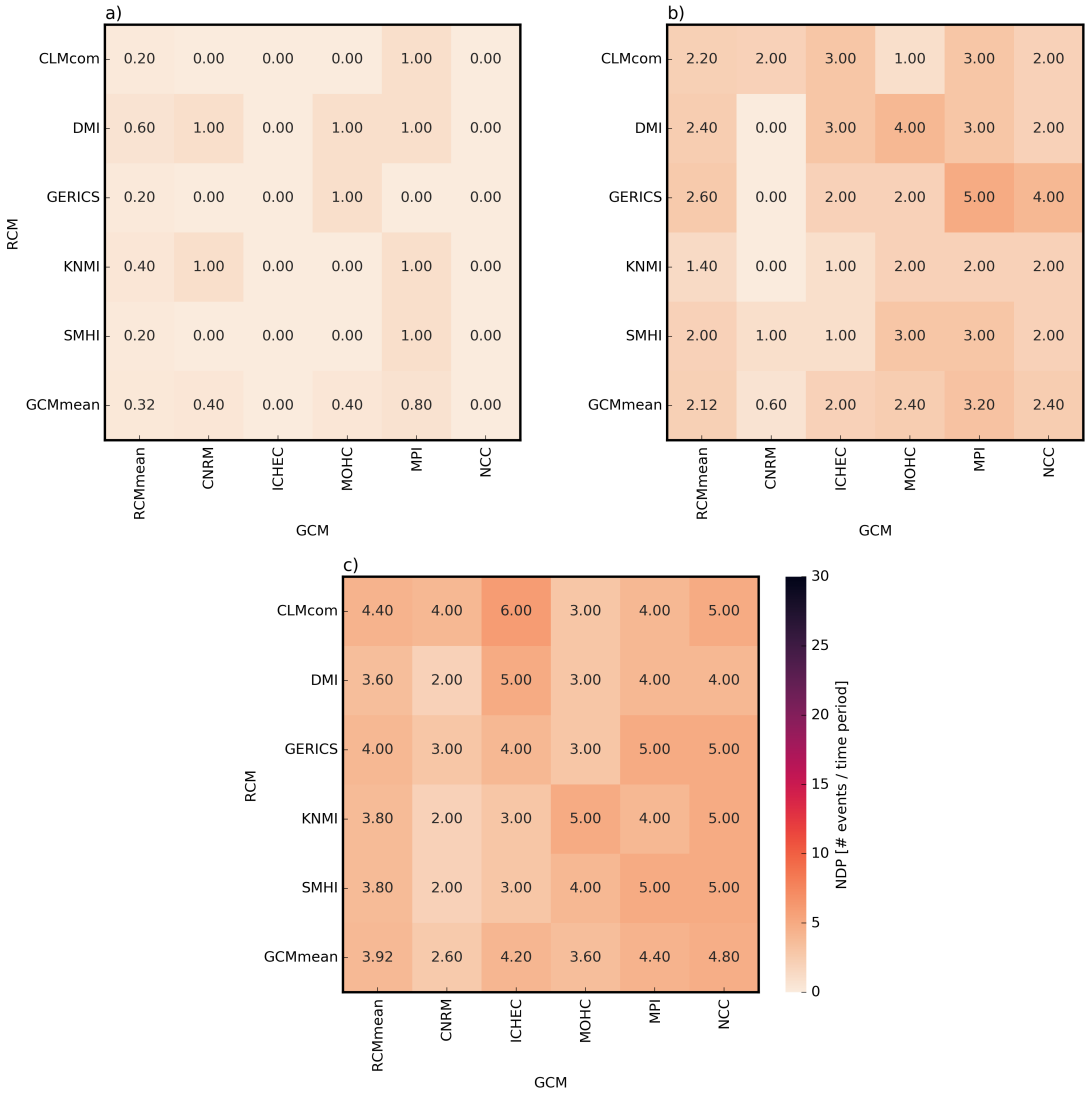

Figure 4.14: Number of Drought Periods (NDP) in the IP a) for the reference period (1971-2000), b) for the NF (2021-2050) and c) for the DF (2071-2100). The table is structured like Fig. 4.3.

frequency to rise in the DF. The highest NDP value is 6, the lowest is 2. Even though the pattern seems rather unstructured, GCMs have a higher spread. HadGEM2-ES, which was the GCM with the strongest drying signal in Fig. 4.3 and Fig. 4.10, has relatively low values. This effect can be understood when considering the high CDY values, that originate from an absence of non-drought years. When drought streaks are not interrupted, only a small number of events can be counted and subsequently NDP values are low. EC-EARTH is the GCM with the biggest frequency in RD events in the DF, which is surprising as it did not show a particularly strong climate change signal in other indices.

The model ensemble projects an increase in RD frequency for both future periods compared to the reference period (significant). GCMs have a slightly higher influence on NDP values than RCMs. The increase in RD frequency is stronger for the DF, if RD duration does not increase so much that it decreases RD frequency.

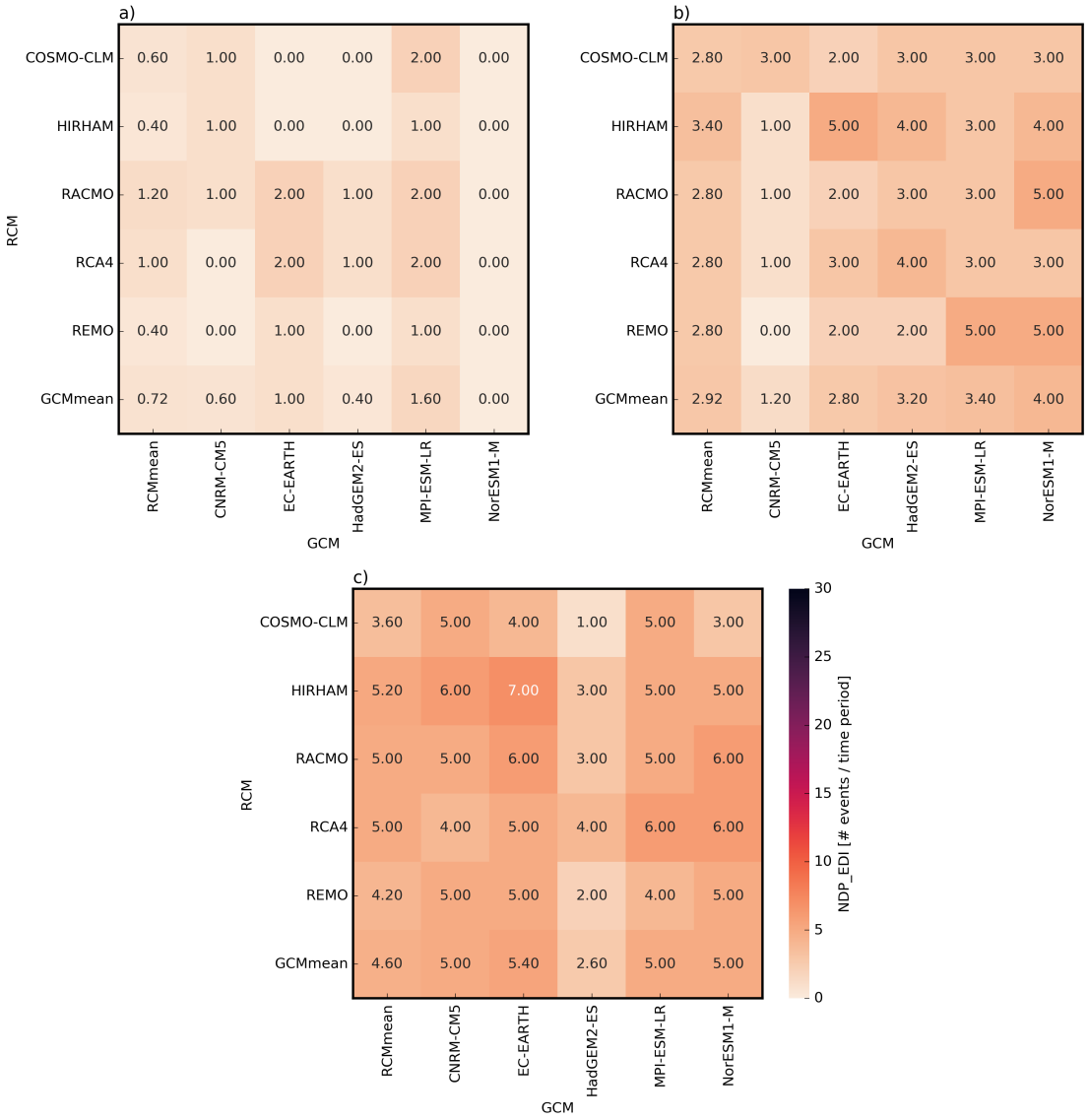

Figure 4.15: Number of Drought Periods based on EDI (NDP_EDI) in the IP a) for the reference period (1971-2000), b) for the NF (2021-2050) and c) for the DF (2071-2100). The table is structured like Fig. 4.3.

Changes in RD frequency and the underlying characteristics of ensemble members are further investigated with the NDP_EDI, similar to the NDP.

The results for the whole IP are displayed in Fig. 4.15. During the reference period, the ensemble mean of NDP_EDI is at 0.72, with values ranging from 0 to 2 (Fig. 4.15 a)). In the NF, the ensemble mean increases to 2.92, while values are increasing for 21 of 25 members, and ranging from 0 to 5, shown in Fig. 4.15 b). The runs with CNRM-CM5 as their GCM show only a small drying trend, compared to the other GCMs. Fig. 4.15 c) suggests a further increase for the DF, with an ensemble mean of 4.6. Values range from 1 to 7. The low values of HadGEM2-ES runs in the DF are striking and can be deducted from the strong drying trend and the high values in CDY_EDI. The other GCMs, including CNRM-CM5, produce similar values.

The model agreement in changes of RD frequency is similar in NDP_EDI and NDP (significant). GCMs again seem to have a stronger influence on NDP_EDI than RCMs.

Overall, RD frequency is projected to increase with ongoing climate change. The consistency among indices is similar to that in section 4.3. Rising numbers of RD events and shorter regeneration time in between events would be likely to cause bigger drought related damages in the future. Changes in RD frequency should only be interpreted in conjunction with changes in (maximum) RD duration, because a very strong increase in drought years reduces the number of RD events.

5 Discussion

In this chapter, the results are summarized, interpreted and compared to the findings of previous studies. Furthermore, the used methods are discussed.

In the ensemble mean, maximum RD duration is increasing in the NF and even more so in the DF. Similarly, also RD frequency is increasing with higher values in the DF. The temporal mean EDI in the NF is negative. This trend intensifies in the DF. There is a tendency to more temporal variability in EDI. However, temporal variability in the DF is smaller than in the NF. A trend towards less precipitation under future climate conditions is found for the whole IP. The reduction in precipitation is biggest in spring and autumn and more pronounced in the DF than in the NF.

The spatial mean temporal mean EDI is useful for characterizing the strength of the climate change signal among different ensemble members. NorESM1-M is the GCM with the strongest drying, while CNRM-CM5 has the weakest drying signal. Among RCMs, COSMO-CLM has the driest members, while those of RACMO are relatively wet. Values in other indices can mostly be explained with these characteristics. The magnitude of projected changes varies strongly across ensemble members. It is mostly determined by the GCMs, because of their influence on the large scale flow, and to a lesser degree by the RCMs. All the trends presented for one dimensional indices have significant model agreement for the IP. The trends for two dimensional indices have significant model agreement in large parts of the IP, with the exception of RDYI and NDY in the NF.

Most metrics and models suggest an acceleration of trends with time, as the difference between reference period and NF is smaller than between NF and DF. However, there are exceptions from that: MPI-ESM-LR has a rather steady than accelerating drying trend, best seen in the spatial mean temporal mean EDI. Models with a strong drying trend show a trend reversal from NF to DF in temporal variability of EDI. This is because a further drying in an already arid climate confines the occurrence of precipitation and therefore variations in the EDI. RD frequency is decreasing for ensemble members with a strong drying signal. This is because non drought years become so rare that drought periods have only few interruptions and the number of RD events decreases, while their duration increases. RD frequency therefore should only be analyzed in conjunction with (maximum) RD duration.

In EDI and related indices (CDY_EDI_GP, CDY_EDI, NDP_EDI, NDP_EDI_GP), the regions with strongest drying signals are the mountainous regions. In indices based on relative annual precipitation sum (RDYI, NDY, CDY, NDP), increases in drought conditions are stronger in the southern regions than in the northern regions. These regional changes in sensitivity originate from differences in interannual variability between regions in the reference period. Some ensemble members show stronger drying in the eastern regions, others project a larger change in the western regions.

RDs are projected to increase with ongoing climate change. Most ensemble members suggest a drastic increase in RDs and project an almost permanent state of drought for some locations or even the whole IP in the DF. In some ensemble members however, RDs are increased, but duration and frequency are of similar magnitude as in the reference period. When addressing future RD impact, all of these ensemble members should be treated as possible future trajectories (Guerreiro et al., 2017). The strong drying scenarios of the model ensemble would have severe consequences for ecosystems (Caldeira et al., 2015) and human life in the IP (Iglesias et al., 2009). This is further intensified by the more pronounced drying trends in mountainous areas. These areas have high annual precipitation sums and are of high importance for the water household in the IP. Extreme adaption measures to secure water supply would be inevitable. But also with the more tempered results of some ensemble members, RDs would pose an increased threat to ecosystems and water supply. The impact on the local scale also doesn't just depend on the strength of the drying signal, but on whether adaption techniques like irrigation are already exhausted under the present day climate.

A projected increase in drought risk is consistent with various past studies. A detailed assessment of the results with regard to previous scientific literature is undertaken:

Precipitation output of climate simulations over topographically complex terrain is often problematic (Prein et al., 2016). However, there is no obvious physical reason for why trends under climate change would be over- or underestimated in mountainous regions. The trends for increased RD changes in mountainous regions are therefore rated as robust. Cardell et al. (2019) came to the conclusion that decreases in seasonal rainfall in Iberia are strongest in spring and autumn, which is consistent with the obtained signal in the annual cycle. Both CNRM-CM5 and MPI-ESM-LR are analyzed in Santos et al. (2016) and their differences in weather type changes suggest that MPI-ESM-LR has a stronger drying trend than CNRM-CM5, which is confirmed in this study. Guerreiro et al. (2017) show an increase in droughts in all models, however with big differences in magnitude. CNRM-CM5 and EC-EARTH register a smaller incline in drought severity than MPI-ESM-LR and HadGEM2-ES, which is consistent with my findings. Also, the models that have a strong signal in drought, show a strong evolution in the drought severity index towards the end of the 21st century, similar to the development in maximum drought duration in my results. According to Spinoni et al. (2018), drought severity, which is well related to drought duration, is increasing with time. For the distant future, all models agree on an intensification of drought conditions. Also, the trend in drought severity is strengthening for a far future time window, all of which is matching my results. Furthermore, they expect droughts in the IP to be roughly 50 % more frequent. The relative changes in RD frequency and maximum duration in this thesis are of even bigger magnitude. However, the nature of the RD indices does not allow for a reasonable comparison in this case, which is further examined in this section. Overall, the results are in agreement with the scientific consensus of drought development in the IP under climate change.

The assessment of RDs in this thesis is adding knowledge on vulnerabilities in the context of climate change in the IP. This will help to obtain a more precise image of climate change impact and support adaption measures. Also, the use of the model ensemble and comparison of single ensemble members improves the understanding of model characteristics in regional climate simulations. The model ensemble is run under the RCP8.5 scenario, which is only one of several scenarios used in CMIP5. It is chosen based on a trade off of availability of simulation data and an evaluation of

recent emission trends. However, future greenhouse gas emission pathways can not be predicted. The usage of different RCP scenarios would be useful to address the sensitivity of RD changes to greeenhouse gas emissions.

Temperature dependent drought indices are disregarded for this analysis in section 2.2.4 to avoid an overestimation of the drying signal (Milly and Dunne, 2017). The results therefore only account for drought changes as consequence of changes in precipitation and lack a signal from temperature increases. Subsequently, the drying trends could be underestimated. An analysis with temperature dependent drought indices could be complementing the results of this thesis.

Because of typical shortcomings in the representation of physical processes, climate simulations are subject to uncertainty (Liang et al., 2008). Future model generations could produce improve results, especially due to increased resolution in time and space.

The applied bias correction method relies on the assumption that the relationship of model world and real world do not change over time, which can not be fully validated. Investigating a potential sensitivity of the results to the bias correction method could add robustness to the results. However, the method applied here does not produce unrealistic values, does not eliminate the variability of ensemble members and produces results that are similar to that of other studies, even in single model characteristics. Therefore, this bias correction approach should be sufficient for investigating the specified drought properties. Because of the dependence on the observational data, robustness of the results could be further increased by using different data sets for bias correction.

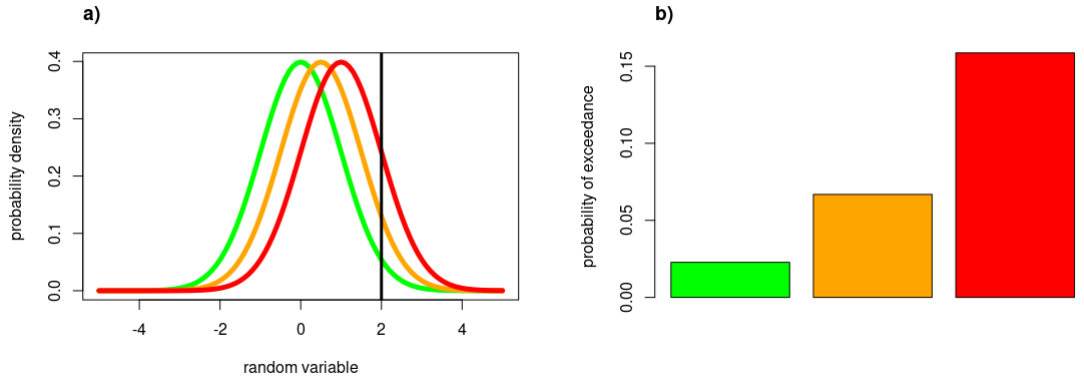

Figure 5.1: Illustration of a) changes in mean (0 for the green, 0.5 for the orange and 2 for the red Probability Distribution Function) of a normally distributed variable b) and subsequent changes in probability of exceedence of a treshold (2).

The RD indices developed in Moemken and Pinto (2021) address ecosystem impact, as described in (Caldeira et al., 2015). They are not meant to describe the rate of change in the physical processes driving climate change. A simplified thought experiment and Fig. 5.1 helps to clarify their non linear reaction on changes in precipitation amounts: The definition of a dry year or drought year is, among others, depending on a normally distributed variable (annual precipitation sum or number of days per year with EDI below -1) remaining below (exceeding) a prescribed treshold, that is smaller (higher) than average. This treshold is depicted by the black line in Fig. 5.1 a) . A linear trend in the mean of the variable towards that treshold is represented by th shift in the mean of the green, orange and red Probability Density Function (PDF) in Fig. 5.1 a). The increase in number of values fulfilling that criterion is not linear, but accelerating. This

is portrayed by the green, orange and red bar in Fig. 5.1 b), where the difference in probability of exceedance between the red and the orange bar is bigger than between the orange and the green bar. The frequency of exceedances of course is just a first step in the calculation of the RD indices. The increase in the maximum number of consecutive exceedances and number of at least two exceedances in a row introduces even more non linearities with regard to a change in the distribution mean, and examining those relationships goes beyond the scope of this thesis. Subsequently, the strong increase in RD indices for the DF compared to the NF should not be interpreted as a sudden acceleration in the rate of climate change, but as a sudden aggravation of climate change impact.

6 Conclusion

Drought is an environmental disaster that is depicted by a lack of water in one or more components of the hydrological cycle (Mishra and Singh, 2010; McKee et al., 1993). Droughts have a particularly high impact in the IP (Iglesias et al., 2009; Gu et al., 2020). Increased drought risk in the Mediterranean as consequence of climate change has wide agreement in scientific literature (Collins et al., 2013; Spinoni et al., 2018; Santos et al., 2016; Guerreiro et al., 2017). Caldeira et al. (2015) suggest that recurrent droughts have a strong impact on ecosystem functioning and tipping points for land degradation. This thesis is the first analysis of these high impact events in regional climate projections. The use of 25 high resolution (0.11°) ensemble members of the EURO-CORDEX project, driven under the RCP8.5 scenario, is aiming to provide an overview of possible developments of recurrent drought risk under future climate conditions. The following are the major results:

• Recurrent droughts are projected to become longer and more frequent under future climate conditions in the IP. In the period from 2071-2100, the IP could face an almost permanent state of drought.

• A general trend of mean conditions towards drought is projected. The temporal variability of dry and wet periods generally increases.

• The model ensemble shows wide agreement for an increased risk of recurrent droughts. The majority of trends have significant model agreement in the 2021-2050 period and the vast majority of trends have significant model agreement for the 2071-2100 period. The magnitude of change varies across models. While some projections indicate rather moderate changes, the majority of them suggest a drastic increase in recurrent drought risk under future climate conditions.

•Variations in drought trends between ensemble members are mainly driven by the GCMs and to a lesser degree by the RCMs. This is because precipitation is strongly related to the large scale flow, which is determined by the GCM.

•The region of biggest increases in recurrent drought risk varies among ensemble members and indeces.

By analyzing recurrent drought, this thesis is deepening the understanding of climate change related drought impact, which is crucial to the implementation of adaption strategies. Furthermore, a detailed picture of variations in drying trends among regional climate simulations is provided.

Climate simulations have typical shortcomings, which introduce uncertainties to the obtained results. Future model generations with improved representation of relevant physical processes could reduce these uncertainties. The analysis in this thesis was carried out with indices that use precipitation as only input variable. Under the premise of sufficient data availability, an analysis with temperature dependent indices could add knowledge on recurrent drought changes under future climate conditions. Further improvements in the robustness of the results could be realized by using different RCP scenarios, bias correction methods and reference data sets.

The increase in recurrent drought risk identified in this analysis would have severe consequences for ecosystems and the population of the IP. Extreme adaption strategies would be required to secure the water supply. From this background, the RCP8.5 scenario presents an highly undesirable pathway for the IP.

A Abbreviations

CDY Consecutive Drought Year Index

CDY_EDI Consecutive Drought Year Index based on EDI

CDY_EDI_GP Consecutive Drought Year Index based on EDI at single Grid Points

DF Distant Future (2071-2100)

DI Drought Index

EDI Effective Drought Index

E-OBS ENSEMBLES daily gridded observational data set

EURO-CORDEX European Branch of the Coordinated Regional Downscaling Experiment

GCM Global Climate Model

IP Iberian Peninsula

IPCC Intergovernmental Panel on Climate Change

NDP Number of Drought Periods

NDP_EDI Number of Drought Periods based on EDI

NDP_EDI_GP Number of Drought Periods based on EDI at single Grid Points

NDY Number of Dry Periods

NF Near Future (2021-2050)

RCM Regional Climate Model

RCP Representative Concentration Pathway

RD Recurrent Drought

RDYI Recurrent Dry Year Index

B Appendix

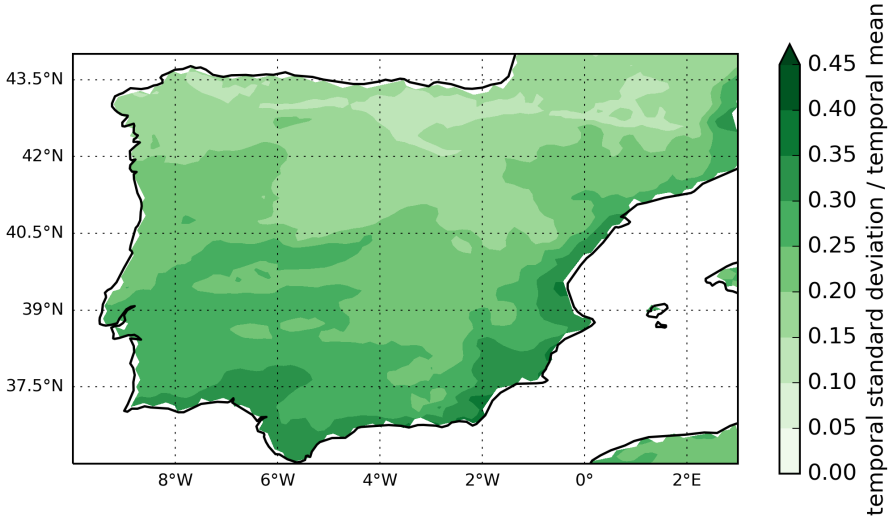

Figure B.1: Ratio between temporal standard deviation and mean of annual precipitation sum of ensemble mean in the reference period (1971-2000).

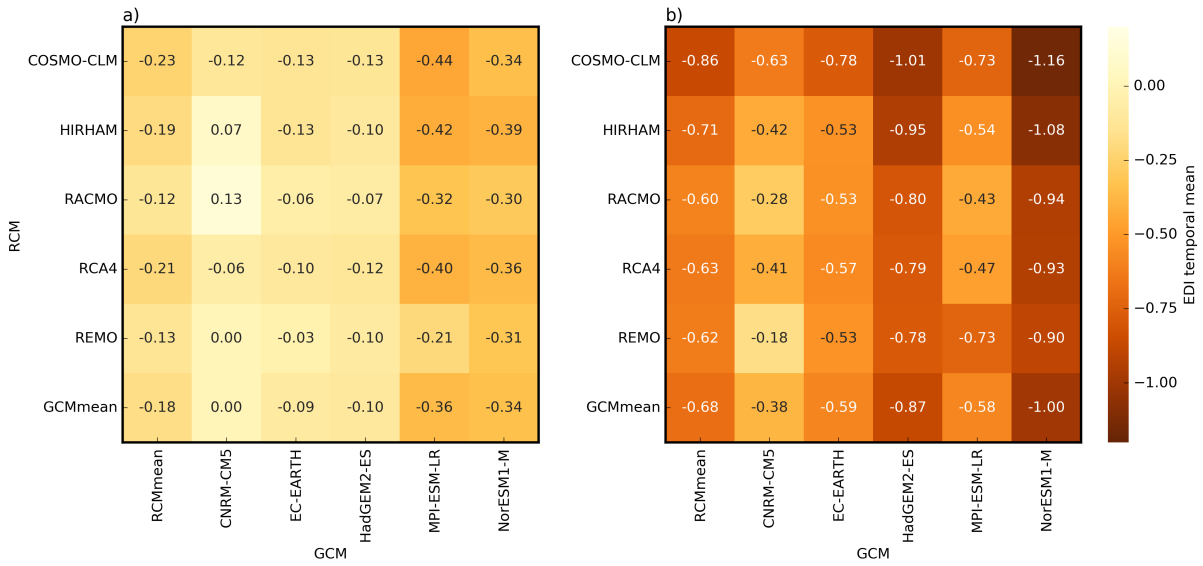

Figure B.2: same as Fig. 4.3, but for IP-NW (40°N to 44°N, 10°W to 5°W).

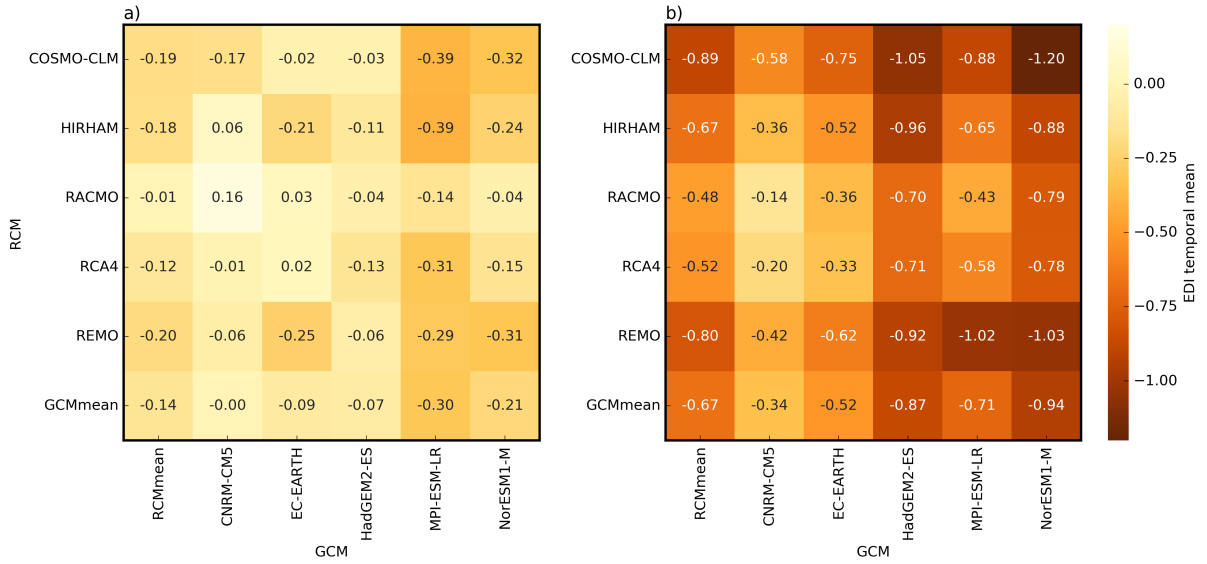

Figure B.3: same as Fig. 4.3, but for IP-NE (40°N to 44°N, 5°W to 0°E).

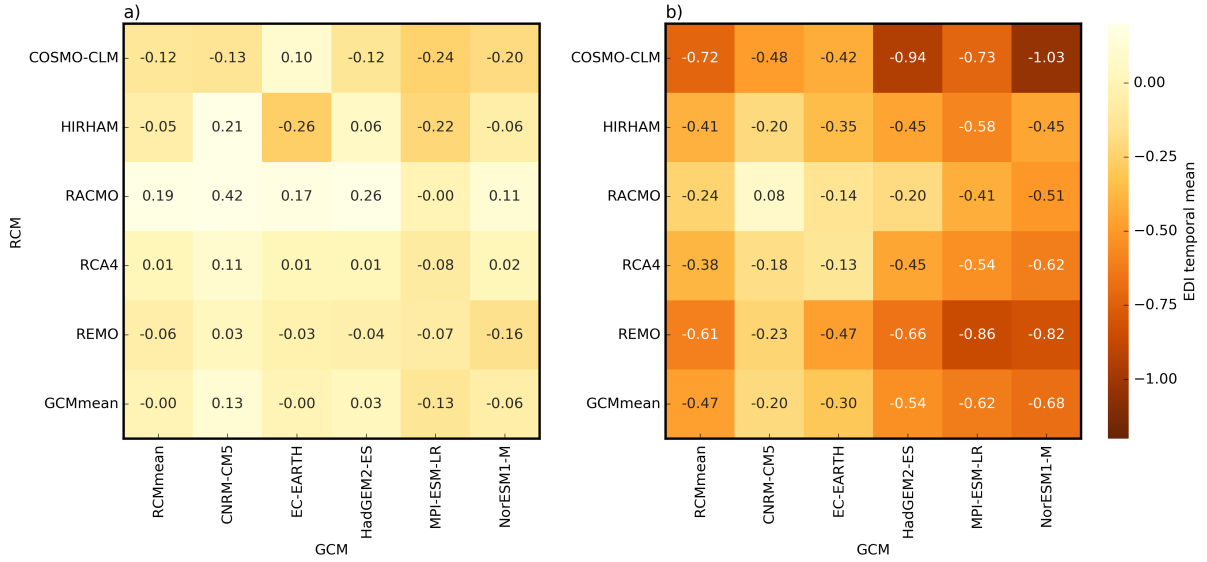

Figure B.4: same as Fig. 4.3, but for IP-E (38°N to 44°N, 0°E to 3°E).

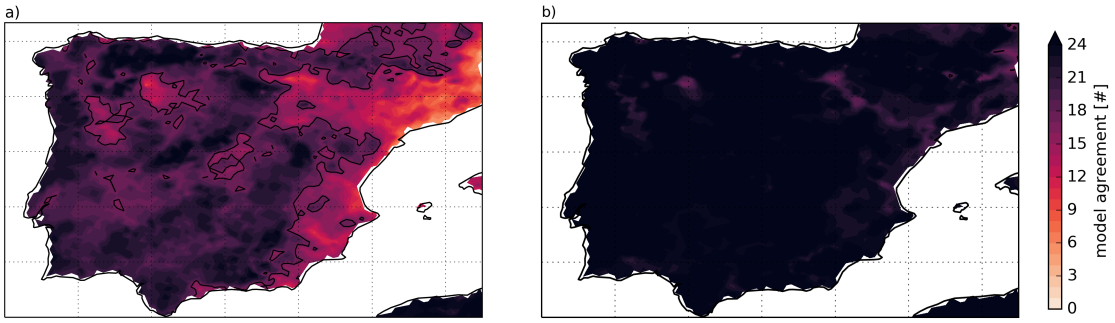

Figure B.5: Effective Drought Index (EDI), temporal mean, model agreement in shading and level of significance (17 of 25 models) as contour line a) for the NF (2021-2050) and b) for the DF (2071-2100).

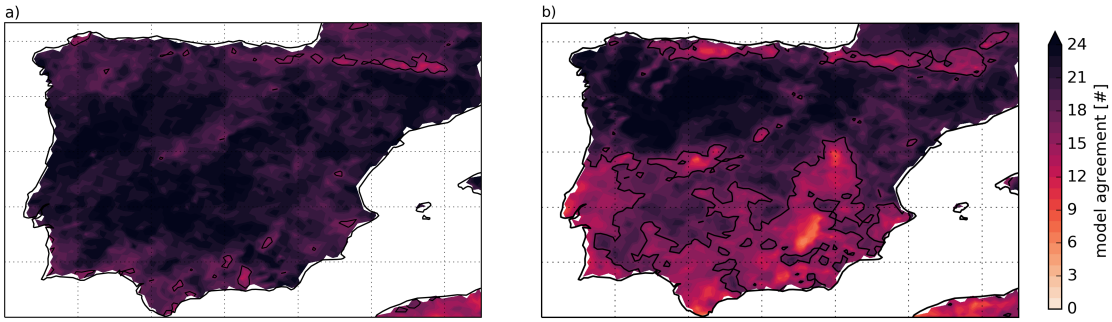

Figure B.6: Same as Fig. B.5 but for temporal standard deviation of Effective Drought Index (EDI).

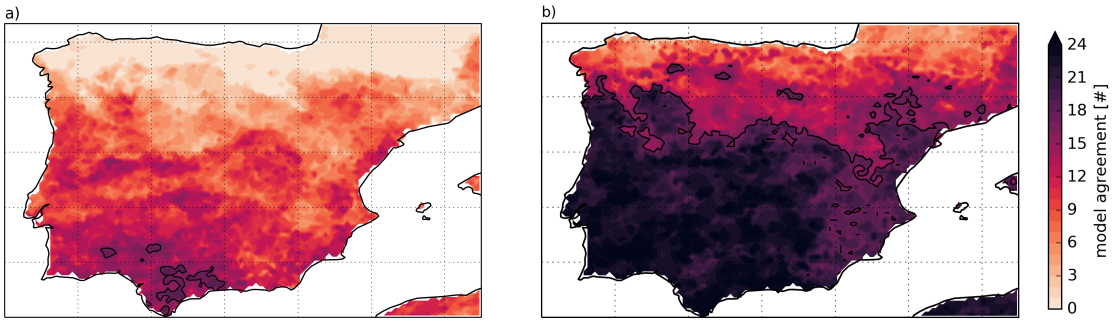

Figure B.7: Same as Fig. B.5 but for Recurrent Dry Year Index (RDYI).

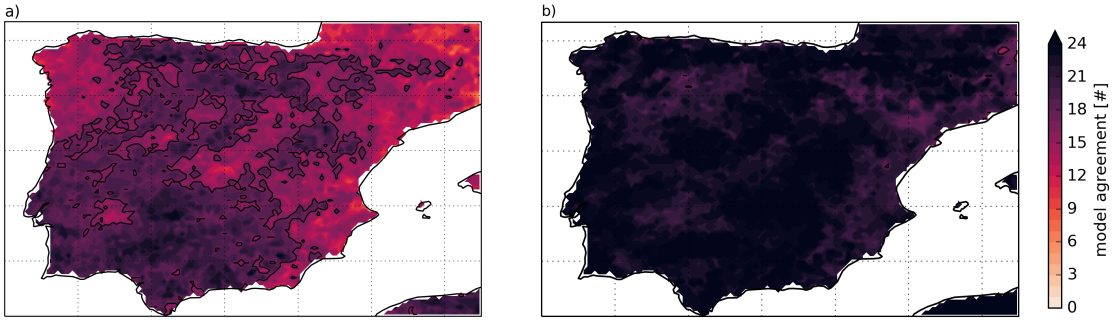

Figure B.8: Same as Fig. B.5 but for Consecutive Drought Year Index based on EDI at single Grid Points (CDY_EDI_GP).

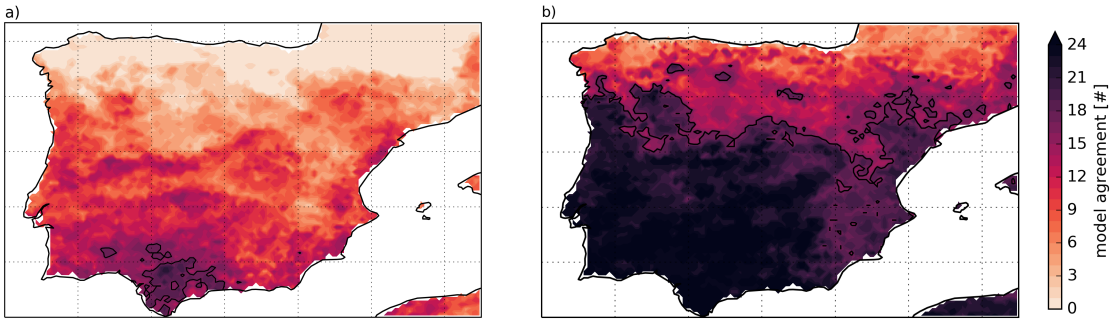

Figure B.9: Same as Fig. B.5 but for Number of Dry Periods (NDY).

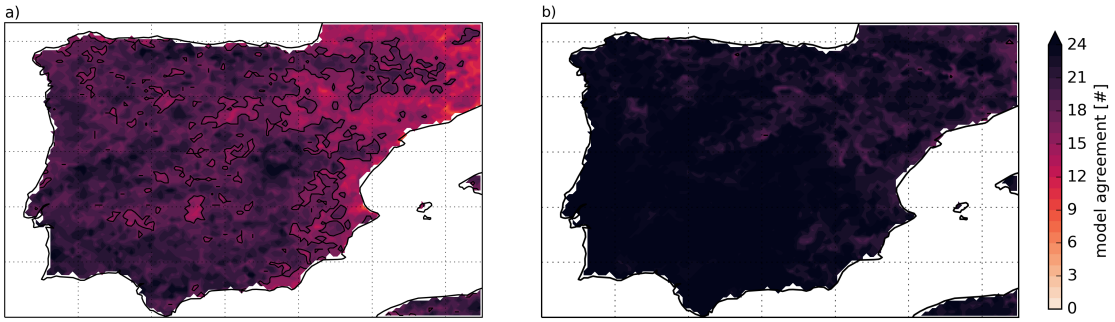

Figure B.10: Same as Fig. B.5 but for Number of Drought Periods based on EDI at single Grid Points (NDP_EDI_GP).

Bibliography

Adaawen, S., and B. Schraven, 2019: The challenges of "drought migration". *German Development Institute*, URL `https://www.die-gdi.de/en/the-current-column/article/the-challenges-of-drought-migration/ (accessed 6 April 2021)`.

Berg, P., H. Feldmann, and H.-J. Panitz, 2012: Bias correction of high resolution regional climate model data. *Journal of Hydrology*, **448-449**, 80–92, doi:10.1016/j.jhydrol.2012.04.026.

Brogli, R., N. Kröner, S. L. Sørland, D. Lüthi, and C. Schär, 2019: The Role of Hadley Circulation and Lapse-Rate Changes for the Future European Summer Climate. *Journal of Climate*, **32 (2)**, 385–404, doi:10.1175/JCLI-D-18-0431.1.

Buchal, C., and C. Schönwiese, 2010: Die Physik der Atmosphaere. *Klima.* MOHN Media Mohndruck GmbH, Guetersloh, 30-65 pp.

Byun, H., and D. Kim, 2010: Comparing the Effective Drought Index and the Standardized Precipitation Index. In Lopez-Francos A. (comp.), Lopez-Francos A. (collab.). Economics of drought and drought preparedness in a climate change context. Zaragoza: CIHEAM / FAO / ICARDA / GDAR / CEIGRAM / MARM. 85–89, URL `https://om.ciheam.org/om/pdf/a95/00801330.pdf`.

Byun, H.-R., and D. A. Wilhite, 1999: Objective Quantification of Drought Severity and Duration. *Journal of Climate*, **12 (9)**, 2747–2756, doi:10.1175/1520-0442(1999)012<2747:OQODSA>2.0.CO;2.

Caldeira, M. C., X. Lecomte, T. S. David, J. G. Pinto, M. N. Bugalho, and C. Werner, 2015: Synergy of extreme drought and shrub invasion reduce ecosystem functioning and resilience in water-limited climates. *Scientific Reports*, **5**, doi:10.1038/srep15110.

Cardell, M., R. Romero, A. Amengual, V. Homar Santaner, and C. Ramis, 2019: A quantile-quantile adjustment of the EURO-CORDEX projections for temperatures and precipitation. *International Journal of Climatology*, **39**, doi:10.1002/joc.5991.

Coll, J., E. Aguilar, and L. Ashcroft, 2017: Drought variability and change across the Iberian Peninsula. *Theoretical and Applied Climatology*, **130**, 901–916, doi:10.1007/s00704-016-1926-3.

Collins, M., and Coauthors, 2013: Long-term Climate Change: Projections, Com-mitments and Irreversibility. In: . *Climate Change 2013: The Physical Science Basis. Contribution of Working Group I to the Fifth Assessment Report of the Intergovernmental Panel on Climate Change*

[Stocker, T.F., D. Qin, G.-K. Plattner, M. Tignor, S.K. Allen, J. Boschung, A. Nauels, Y. Xia, V. Bex and P.M. Midgley (eds.)]. Cambridge University Press, Cambridge, United Kingdom and New York, NY, USA.

Comas-Bru, L., and F. McDermott, 2014: Impacts of the EA and SCA patterns on the European twentieth century NAO–winter climate relationship. *Quarterly Journal of the Royal Meteorological Society*, **140 (679)**, 354–363, doi:10.1002/qj.2158.

Cornes, R. C., G. van der Schrier, E. J. M. van den Besselaar, and P. D. Jones, 2018: An Ensemble Version of the E-OBS Temperature and Precipitation Data Sets. *Journal of Geophysical Research: Atmospheres*, **123 (17)**, 9391–9409, doi:10.1029/2017JD028200.

Deo, R., H. Byun, J. Adamowski, and K. Begum, 2017: Application of effective drought index for quantification of meteorological drought events: a case study in Australia. *Theoretical and Applied Climatology*, **128**, 359–379, doi:10.1007/s00704-015-1706-5.

Esteban-Parra, M. J., F. S. Rodrigo, and Y. Castro-Diez, 1998: Spatial and temporal patterns of precipitation in Spain for the period 1880–1992. *International Journal of Climatology*, **18 (14)**, 1557–1574, doi:10.1002/(SICI)1097-0088(19981130)18:14<1557::AID-JOC328>3.0.CO;2-J.

García-Herrera, R., E. Hernández, D. Barriopedro, D. Paredes, R. M. Trigo, I. F. Trigo, and M. A. Mendes, 2007: The Outstanding 2004/05 Drought in the Iberian Peninsula: Associated Atmospheric Circulation . *Journal of Hydrometeorology*, **8 (3)**, 483–498, doi:10.1175/JHM578.1.

Giorgi, F., C. Jones, and G. Asrar, 2008: Addressing climate information needs at the regional level: The CORDEX framework. *WMO Bull*, **53**, URL `https://public.wmo.int/en/bulletin/addressing-climate-information-needs-regional-level-cordex-framework`.

Goodess, C. M., and P. D. Jones, 2002: Links between circulation and changes in the characteristics of Iberian rainfall. *International Journal of Climatology*, **22 (13)**, 1593–1615, doi:10.1002/joc.810.

Gu, L., J. Chen, J. Yin, S. C. Sullivan, H.-M. Wang, S. Guo, L. Zhang, and J.-S. Kim, 2020: Projected increases in magnitude and socioeconomic exposure of global droughts in 1.5° and 2°C warmer climates. *Hydrology and Earth System Sciences*, **24 (1)**, 451–472, doi:10.5194/hess-24-451-2020.

Guerreiro, S., C. Kilsby, and H. Fowler, 2017: Assessing the threat of future megadrought in Iberia. *International Journal of Climatology*, doi:10.1002/joc.5140.

Hamdy, A., G. Trisorio-Liuzzi, and M. Agronomic, 2008: Drought planning and drought mitigation measures in the Mediterranean region. *Options Méditerranéennes*, **A (80)**, 235–239, URL `https://om.ciheam.org/om/pdf/a80/00800448.pdf`.

Hartmann, D., and Coauthors, 2013: Observations: Atmosphere and Surface. In:. *Climate Change 2013: The Physical Science Basis. Contribution of Working Group I to the Fifth Assessment*

Report of the Intergovernmental Panel on Climate Change [Stocker, T.F., D. Qin, G.-K. Plattner, M. Tignor, S.K. Allen, J. Boschung, A. Nauels, Y. Xia, V. Bex and P.M. Midgley (eds.)]. Cambridge University Press, Cambridge, United Kingdom and New York, NY, USA.

Hausfather, Z., and G. B. Peters, 2019: Emissions – the 'business as usual' story is misleading. *nature*, **577**, 618–620, doi:10.1038/d41586-020-00177-3.

Hayes, M., M. Svoboda, N. Wall, and M. Widhalm, 2011: The Lincoln Declaration on Drought Indices: Universal Meteorological Drought Index Recommended. *Bulletin of the American Meteorological Society*, **92**, 485–488, doi:10.1175/2010BAMS3103.1.

Herrera, S., R. M. Cardoso, P. M. Soares, F. Espírito-Santo, P. Viterbo, and J. M. Gutiérrez, 2019: Iberia01: a new gridded dataset of daily precipitation and temperatures over Iberia, journal = Earth System Science Data. **11 (4)**, 1947–1956, doi:10.5194/essd-11-1947-2019.

Herrera, S., J. Fernández, and J. M. Gutiérrez, 2016: Update of the Spain02 gridded observational dataset for EURO-CORDEX evaluation: assessing the effect of the interpolation methodology. *International Journal of Climatology*, **36 (2)**, 900–908, doi:10.1002/joc.4391.

Hofstra, N., M. Haylock, M. New, and P. Jones, 2009: Testing E-OBS European high-resolution gridded data set of daily precipitation and surface temperature. *Journal of Geophysical Research. D, Atmospheres 114 (2009) D21101*, **114**, doi:10.1029/2009JD011799.

Howell, T., and S. Evett, 2004: The Penman-Monteith Method. Section 3 in Evapotranspiration: Determination of Consumptive Use in Water Rights Proceedings. Continuing Legal Education in Colorado, Inc. Denver, CO. URL `https://www.researchgate.net/publication/241492864_The_Penman-Monteith_Method`.

Huffman, G. J., and Coauthors, 2007: The TRMM Multisatellite Precipitation Analysis (TMPA): Quasi-Global, Multiyear, Combined-Sensor Precipitation Estimates at Fine Scales. *Journal of Hydrometeorology*, **8 (1)**, 38–55, doi:10.1175/JHM560.1.

Hurrell, J., Y. Kushnir, G. Ottersen, and M. Visbeck, 2003: *The North Atlantic Oscillation*, Vol. 134. doi:10.1029/134GM01.

Iglesias, A., L. Garrote, and F. Martín-Carrasco, 2009: Drought risk management in mediterranean river basins. *Integrated Environmental Assessment and Management*, **5 (1)**, 11–16, doi:10.1897/IEAM_2008-044.1.

Jacob, D., and Coauthors, 2014: EURO-CORDEX: New high-resolution climate change projections for European impact research. *Regional Environmental Changes*, **14**, doi:10.1007/s10113-013-0499-2.

Kamruzzaman, M., M.-W. Jang, J. Cho, and S. Hwang, 2019: Future Changes in Precipitation and Drought Characteristics over Bangladesh under CMIP5 Climatological Projections . *Water*, **11 (2219)**, doi:10.3390/w11112219.

Khodayar, S., A. Sehlinger, H. Feldmann, and C. Kottmeier, 2015: Sensitivity of soil moisture initialization for decadal predictions under different regional climatic conditions in Europe. *International Journal of Climatology*, **35 (8)**, 1899–1915, doi:https://doi.org/10.1002/joc.4096.

Kim, D.-W., and H.-R. Byun, 2009: Future pattern of Asian drought under global warming scenario. *Theoretical and Applied Climatology*, **98**, 137–150, doi:10.1007/s00704-008-0100-y.

Kirtman, B., and Coauthors, 2013: Near-term Climate Change: Projections and Predictability. In: . *Climate Change 2013: The Physical Science Basis. Contribution of Working Group I to the Fifth Assessment Report of the Intergovernmental Panel on Climate Change* [Stocker, T.F., D. Qin, G.-K. Plattner, M. Tignor, S.K. Allen, J. Boschung, A. Nauels, Y. Xia, V. Bex and P.M. Midgley (eds.)]. Cambridge University Press, Cambridge, United Kingdom and New York, NY, USA.

Lee, B., S. Oh, and H. Byun, 2014: The characteristics of drought occurrence in North Korea and its comparison with drought in South Korea. *Theoretical and Applied Climatology*, **121**, 199–209.

Li, S., L. Li, and H. Le Treut, 2016: Two-way against one-way nesting for climate downscaling in Europe and the Mediterranean region using LMDZ4. *EGU General Assembly Conference Abstracts*, EPSC2016–3125, URL `https://ui.adsabs.harvard.edu/abs/2016EGUGA..18.3125L`.

Liang, X.-Z., K. E. Kunkel, G. A. Meehl, R. G. Jones, and J. X. L. Wang, 2008: Regional climate models downscaling analysis of general circulation models present climate biases propagation into future change projections. *Geophysical Research Letters*, **35 (8)**, doi:10.1029/2007GL032849.

Ludwig, P., J. Gómez-Navarro, J. Pinto, C. Raible, S. Wagner, and E. Zorita, 2019: Perspectives of Regional Paleoclimate Modelling. *Annals of the New York Academy of Sciences*, **1436**, 54–69, doi:10.1111/nyas.13865.

McKee, T. B., N. J. Doesken, and J. Kleist, 1993: The relationship of drought frequency and duration to time scales. *Eigth conference on Applied Climatology*, URL `https://www.droughtmanagement.info/literature/AMS_Relationship_Drought_Frequency_Duration_Time_Scales_1993.pdf`.

Meinshausen, M., and Coauthors, 2011: The RCP greenhouse gas concentrations and their extensions from 1765 to 2300. *Climatic Change*, **109**, 213, doi:10.1007/s10584-011-0156-z.

Milly, P., and K. Dunne, 2017: A Hydrologic Drying Bias in Water-Resource Impact Analyses of Anthropogenic Climate Change. *JAWRA Journal of the American Water Resources Association*, doi:10.1111/1752-1688.12538.

Mishra, A. K., and V. P. Singh, 2010: A review of drought concepts. *Journal of Hydrology*, **391 (1)**, 202–216, doi:10.1016/j.jhydrol.2010.07.012.

Moemken, J., and J. G. Pinto, 2021: Recurrence of historical drought events over Iberia in 1950-2018. *In preparation*.

Moore, G. W. K., I. A. Renfrew, and R. S. Pickart, 15 Apr. 2013: Multidecadal Mobility of the North Atlantic Oscillation. *Journal of Climate*, **26 (8)**, 2453–2466, doi:10.1175/JCLI-D-12-00023.1.

Mukherjee, S., A. Mishra, and K. E. Trenberth, 2018: Climate Change and Drought: a Perspective on Drought Indices. *Current Climate Change Reports*, **4**, 145–163, doi:10.1007/s40641-018-0098-x.

NOAA, and NCEI, 2002: North American Drought Monitor. *National Oceanic and Atmospheric Administration (NOAA) and National Centers for Environmental Information (NCEI)*, URL `https://www.drought.gov/data-maps-tools/north-american-drought-monitor-nadm-indices-and-data (accessed 12 April 2021)`.

Orlowsky, B., and S. I. Seneviratne, 2012: Global changes in extreme events: regional and seasonal dimension. *Climatic Change*, **110**, 669–696, doi:10.1007/s10584-011-0122-9.

Palmer, W. C., 1965: Meteorological Drought. *U.S. Research Paper No. 45*, URL `https://www.ncdc.noaa.gov/temp-and-precip/drought/docs/palmer.pdf`.

Peterson, T., 2005: Climate Change Indices. *WMO Bulletin*, **54 (2)**, 83–86, URL `http://etccdi.pacificclimate.org/papers/WMO.Bulletin.April.2005.indices.pdf`.

Prein, A. F., and Coauthors, 2016: Precipitation in the EURO-CORDEX 0.11° and 0.44° simulations: high resolution, high benefits? *Climate Dynamics*, **46**, 383–412, doi:10.1007/s00382-015-2589-y.

Putnam, A. E., and W. S. Broecker, 2017: Human-induced changes in the distribution of rainfall. *Science Advances*, **3 (5)**, doi:10.1126/sciadv.1600871.

R Core Team, 2017: *R: A Language and Environment for Statistical Computing*. Vienna, Austria, R Foundation for Statistical Computing, URL `https://www.R-project.org/`.

Reilly, J., and Coauthors, 1995: Impacts, Adaptations and Mitigation of Climate Change: Scientific-Technical Analyses: Contribution of Working Group II to the Second Assessment Report of the Intergovernmental Panel on Climate Change, Chapter 13: Agriculture in a Changing Climate: Impacts and Adaptation.

Rodriguez-Puebla, C., A. H. Encinas, S. Nieto, and J. Garmendia, 1998: Spatial and temporal patterns of annual precipitation variability over the Iberian Peninsula. *International Journal of Climatology*, **18 (3)**, 299–316, doi:10.1002/(SICI)1097-0088(19980315)18:3<299::AID-JOC247>3.0.CO;2-L.

Santos, J. A., M. Belo-Pereira, H. Fraga, and J. G. Pinto, 2016: Understanding climate change projections for precipitation over western Europe with a weather typing approach. *Journal of Geophysical Research: Atmospheres*, **121 (3)**, 1170–1189, doi:10.1002/2015JD024399.

Schulzweida, U., 2019: Cdo user guide. URL 10.5281/zenodo.3539275, doi: 10.5281/zenodo.3539275.

Schwalm, C. R., S. Glendon, and P. B. Duffy, 2020: RCP8.5 tracks cumulative CO2 emissions. *Proceedings of the National Academy of Sciences*, **117 (33)**, 19 656–19 657, doi: 10.1073/pnas.2007117117.

Seager, R., H. Liu, N. Henderson, I. Simpson, C. Kelley, T. Shaw, Y. Kushnir, and M. Ting, 2014: Causes of Increasing Aridification of the Mediterranean Region in Response to Rising Greenhouse Gases. *Journal of Climate*, **27 (12)**, 4655 – 4676, doi:10.1175/JCLI-D-13-00446.1.

Shahbazbegian, M., and A. Bagheri, 2010: Rethinking assessment of drought impacts: a systemic approach towards sustainability. *Sustainability Science*, **2**, 223–236, doi:10.1007/s11625-010-0110-4.

Spinoni, J., J. Vogt, G. Naumann, P. Barbosa, and A. Dosio, 2018: Will drought events become more frequent and severe in Europe? *International Journal of Climatology*, **38**, 1718–1736, doi:10.1002/joc.5291.

Stagge, J., L. Tallaksen, C. Xu, and H. Van Lanen, 2014: Standardized precipitation-evapotranspiration index (SPEI): Sensitivity to potential evapotranspiration model and parameters. *Hydrology in a Changing World*, E. Servat, J.-E. Paturel, A. Dezetter, G. Laaha, J.-F. Boyer, D. Ruelland, S. Demuth, G. Mahe, T. Daniell, and H. van Lanen, Eds., Copernicus GmbH, 367–373, IAHS-AISH Proceedings and Reports, URL https://iahs.info/uploads/dms/16617.66-367-373-363-55-Paper-213-Stagge.pdf, 7th World Flow Regimes from International and Experimental Network Data-Water Conference, FRIEND-Water 2014 ; Conference date: 07-10-2014 Through 10-10-2014.

Taylor, K. E., R. J. Stouffer, and G. A. Meehl, 01 Apr. 2012: An Overview of CMIP5 and the Experiment Design. *Bulletin of the American Meteorological Society*, **93 (4)**, 485 – 498, doi: 10.1175/BAMS-D-11-00094.1.

Thornthwaite, C. W., 1948: An approach toward a rational classification of climate. *Geographical Review*, **38 (1)**, 55–94, URL https://www.jstor.org/stable/210739?seq=1.

Trigo, R. M., D. Pozo-Vázquez, T. J. Osborn, Y. Castro-Díez, S. Gámiz-Fortis, and M. J. Esteban-Parra, 2004: North Atlantic oscillation influence on precipitation, river flow and water resources in the Iberian Peninsula. *International Journal of Climatology*, **24 (8)**, 925–944, doi: 10.1002/joc.1048.

Tuel, A., S. Kang, and E. A. B. Eltahir, 2021: Understanding climate change over the southwestern Mediterranean using high-resolution simulations. *Climate Dynamics*, **56**, 985–1001, doi:10.1007/s00382-020-05516-8.

UNDP, 2015: World leaders adopt Sustainable Development Goals. *United Nations Development Programme*, URL http://www.undp.org/content/undp/en/home/presscenter/pressreleases/2015/

09/24/undp-welcomes-adoption-of-sustainable-development-goals-by-world-leaders.html (accessed 6 April 2021).

Van Engelen, A., A. Klein Tank, G. van der Schrier, and L. Klok, 2008: European Climate Assessment Dataset (ECAD), Report 2008. KNMI. URL https://www.ecad.eu/documents/ECAD_report_2008.pdf.

Van Rossum, G., and F. L. Drake, 2009: Python 3 Reference Manual. CreateSpace, Scotts Valley, CA.

Vicente-Serrano, S., S. Beguería, and J. López-Moreno, 2010: A Multiscalar Drought Index Sensitive to Global Warming: The Standardized Precipitation Evapotranspiration Index. *Journal of Climate*, **23**, 1696–1718, doi:10.1175/2009JCLI2909.1.

Vicente-Serrano, S. M., and Coauthors, 2014: Evidence of increasing drought severity caused by temperature rise in southern Europe. *Environmental Research Letters*, **9 (4)**, doi:10.1088/1748-9326/9/4/044001.

Wallace, J. M., and D. S. Gutzler, 1981: Teleconnections in the Geopotential Height Field during the Northern Hemisphere Winter. *Mon. Wea. Rev.*, **109**, 784–812, doi:10.1175/1520-0493(1981)109<0784:TITGHF>2.0.CO;2.

Wells, N., S. Goddard, and M. J. Hayes, 2004: A Self-Calibrating Palmer Drought Severity Index. *Journal of Climate*, **17 (12)**, 2335–2351, doi:10.1175/1520-0442(2004)017<2335:ASPDSI>2.0.CO;2.

Wilhite, D. A., 1992: *Drought* Encyclopedia of Earth System Science, vol. 2. San Diego: Academic Press, 1992, 81-92 pp.

Wilhite, D. A., M. J. Hayes, and M. Svoboda, 2007: Understanding the Complex Impacts of Drought: A Key to Enhancing Drought Mitigation and Preparedness. *Water Resources Management*, doi:10.1007/s11269-006-9076-5.

Wilhite, D. A., M. V. Sivakumar, and R. Pulwarty, 2014: Managing drought risk in a changing climate: The role of national drought policy. *Weather and Climate Extremes*, **3**, 4–13, doi:10.1016/j.wace.2014.01.002.

WMO, 2006: Drought Monitoring and Early Warning: Concepts, Progress, and Future Challenges. WMO-No.1006, World Meteorological Organization, Geneva, Switzerland. URL https://www.droughtmanagement.info/literature/WMO_drought_monitoring_early_warning_2006.pdf.

Yang, X., E. Wood, J. Sheffield, L. Ren, M. Zhang, and Y. Wang, 2018: Bias Correction of Historical and Future Simulations of Precipitation and Temperature for China from CMIP5 Models. *Journal of Hydrometeorology*, **19**, doi:10.1175/JHM-D-17-0180.1.

Zender, C. S., 2014: *netCDF Operator (NCO) User Guide, Version 4.4.8*. URL http://nco.sf.net/nco.pdf.

Zhang, X., L. Alexander, G. C. Hegerl, P. Jones, A. K. Tank, T. C. Peterson, B. Trewin, and F. W. Zwiers, 2011: Indices for monitoring changes in extremes based on daily temperature and precipitation data. *Wiley Interdisciplinary Reviews: Climate Change*, **2 (6)**, 851–870, doi: 10.1002/wcc.147.

Danksagung

Nun möchte ich mich noch bei den Menschen bedanken, die das Erreichen des Masterabschlusses und die Anfertigung dieser Masterarbeit ermöglicht haben.

Bedanken möchte ich mich bei Prof. Dr. Joaquim Pinto, der der Referent dieser Arbeit ist. Die regelmäßigen Besprechungen und die fachliche Beratung hat mich in meiner Forschung stets unterstützt.

Ebenfalls bedanke ich mich bei dem Koreferenten Prof. Dr. Andreas Fink, der durch seine wissenschaftliche Erfahrung ebenfalls zum Gelingen dieser Arbeit beigetragen hat.

Für eine sehr engagierte Betreuung danke ich Dr. Julia Mömken. Ohne die zahlreichen Meetings, die technische Unterstützung, die konstruktive Kritik und den freundlichen Umgang wäre diese Arbeit so nicht zustande gekommen.

Für viel technische und fachliche Unterstützung und großen Einsatz geht mein Dank an Hendrik Feldmann und Dr. Florian Ehmele. Auch bei den übrigen Mitgliedern der Arbeitsgruppe 'Regionales Klima und Wettergefahren' möchte ich gerne für ihre Ideen und Hilfe danken.

Zuletzt geht für Unterstützung auf vielfältige Weise auch ein Dankeschön an Kommiliton*innen, Freunde und Verwandte.

Vielen herzlichen Dank!

Erklärung

Ich versichere wahrheitsgemäß, die Arbeit selbstständig angefertigt, alle benutzten Hilfsmittel vollständig und genau angegeben und alles kenntlich gemacht zu haben, was aus Arbeiten anderer unverändert oder mit Abänderungen entnommen.
Ich versichere wahrheitsgemäß, die Arbeit selbstständig verfasst, alle benutzten Hilfsmittel vollständig und genau angegeben und alles kenntlich gemacht zu haben, was aus Arbeiten anderer unverändert oder mit Abänderungen entnommen wurde sowie die Satzung des KIT zur Sicherung guter wissenschaftlicher Praxis in der jeweils gültigen Fassung beachtet zu haben.

Karlsruhe, den 08. 04. 2021

Benjamin Körner